SRSA: SKILL RETRIEVAL AND ADAPTATION FOR ROBOTIC ASSEMBLY TASKS

Anonymous authors
Paper under double-blind review

ABSTRACT

Enabling robots to learn novel tasks in a data-efficient manner is a long-standing challenge. Common strategies involve carefully leveraging prior experiences, especially transition data collected on related tasks. Although much progress has been made in developing such strategies for general pick-and-place manipulation, far fewer studies have investigated contact-rich assembly tasks, where precise control is essential. In this work, we present **SRSA** (**S**kill **R**etrieval and **S**kill **A**daptation), a novel framework designed to address this problem by utilizing a pre-existing skill library containing policies for diverse assembly tasks. The challenge lies in identifying which skill from the library is most relevant for fine-tuning on a new task. Our key hypothesis is that skills showing higher zero-shot success rates on a new task are better suited for rapid and effective fine-tuning on that task. To this end, we propose to predict the transfer success for all skills in the skill library on a novel task, and then use this prediction to guide the skill retrieval process. Through extensive experiments, we demonstrate that SRSA significantly outperforms the leading baseline, achieving a 22% relative improvement in success rate, 3.7x higher stability, and 2.4x greater sample efficiency when retrieving and fine-tuning skills on unseen tasks. Moreover, in a continual learning setup, SRSA efficiently learns policies for new tasks and incorporates them into the skill library, enhancing future policy learning. Additionally, policies trained with SRSA in simulation achieve a 90% mean success rate when deployed in the real world. Please visit our project webpage at `https://srsa2024.github.io/` for videos.

1 INTRODUCTION

Humans excel at solving new tasks with few demonstrations or trial-and-error interactions. In robot learning, a key challenge is to similarly enable robots to learn control policies from sensor-based observations in a data-efficient manner. Achieving data-efficient learning is crucial for deploying robots in diverse real-world environments, such as the household and industry. A compelling approach to efficient policy learning is the development of a foundation model or generalist policy that spans multiple tasks because it offers long-term efficiency gains by providing a strong base for adaptation to novel tasks. Significant advancements have been made in manipulation tasks, particularly in visual pre-training (Parisi et al., 2022; Nair et al., 2022), multi-task policy learning (Shridhar et al., 2022; Goyal et al., 2024), and policy generalization (Jang et al., 2022; Ebert et al., 2021).

Despite this progress, efficiently solving new tasks in contact-rich environments, such as robotic assembly, remains underexplored. Robotic assembly plays a critical role in industries like automotive, aerospace, and electronics, but learning assembly policies is uniquely difficult. These tasks require contact-rich interactions with high levels of precision and accuracy, compounded by the physical complexity of the environments, part variability, and strict reliability standards. Much of the existing research focuses on training specialist (i.e., single-task) policies for individual assembly tasks (Spector & Di Castro, 2021; Spector et al., 2022; Tang et al., 2023). Building on the strengths of these specialist approaches, we propose a novel method for tackling new assembly tasks. Our approach leverages a skill library – a collection of diverse specialist policies and associated information (such as object geometry and task-relevant trajectories) for various assembly tasks. These policies and data, regardless of the training strategies or learning approaches used to develop them, can be harnessed to efficiently solve previously-unseen assembly challenges.

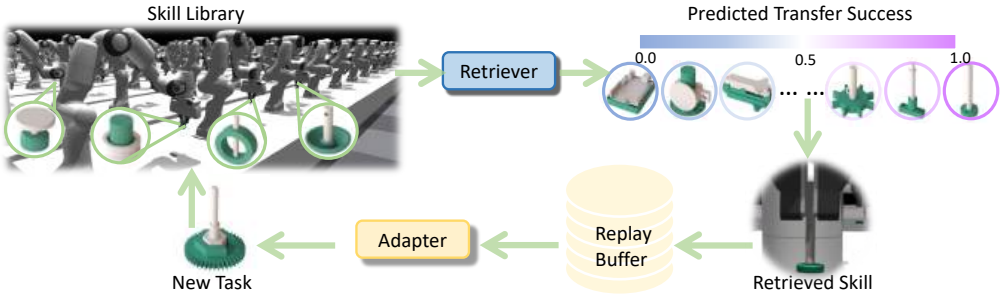

Figure 1: **Overview of SRSA.** We address assembly tasks, where the goal is to use a robot arm to insert diverse *plugs* (i.e., the white parts) into or onto corresponding *sockets* (i.e., the green parts). Specifically, we propose to predict the transfer success of applying prior skills (i.e., policies) to a new task, retrieve the skill with the highest predicted success rate, and fine-tune it on the new task. During fine-tuning, we accelerate and stabilize adaptation by incorporating imitation learning of high-rewarding transitions from the agent's own replay buffer.

To utilize prior task experiences, previous work on general pick-and-place tasks has explored methods such as imitating state-action pairs from expert demonstrations (Du et al., 2023; Lin et al., 2024; Kuang et al., 2024) and encoding sub-task skills as macro-action choices (Lynch et al., 2020; Pertsch et al., 2021; Nasiriany et al., 2022). Unlike these approaches, which focus on reusing data or sub-task skills, our approach centers on adapting *policies* from previous tasks to solve novel tasks. These policies encapsulate essential task-solving knowledge in a generative form, making them a valuable starting point for further refinement. Despite having access to a library of policies, identifying the most relevant ones for fine-tuning on new tasks is still an open question, and the success of fine-tuning hinges on making the right selection. In this paper, we introduce **SRSA** (**S**kill **R**etrieval and **S**kill **A**daptation), a novel framework designed to retrieve policies for similar tasks and adapt them to new tasks, as illustrated in Fig. 1. The key contributions of this paper are as follows:

(1) Skill Retrieval Method: We propose a skill retrieval method that simultaneously and explicitly learns embeddings for three fundamental components of assembly tasks: part geometry, interaction dynamics, and expert action choices. We subsequently introduce a novel objective that leverages these embeddings to predict transfer success across any source policy and target task, implicitly capturing additional critical factors for policy transfer. This approach enables the effective retrieval of relevant skills, resulting in higher zero-shot transfer success when applied to new tasks.

(2) Skill Adaptation Method: We propose a skill adaptation method that fine-tunes retrieved skills on new tasks while incorporating a self-imitation learning method (Oh et al., 2018) to enhance performance and stability during fine-tuning. In a simulation-based, dense-reward setting explored in the leading assembly baseline (Tang et al., 2024), SRSA achieves a relative improvement of 22% in success rate with 2.4x faster training and 3.7x greater stability. In simulation-based, sparse-reward settings without demonstrations or curriculum (closely aligning with real-world fine-tuning scenarios), SRSA outperforms the baseline with a relative improvement of 139% in success rate. Furthermore, we demonstrate that policies fine-tuned in simulation can be directly transferred to real-world robots, achieving a 90% average success rate without the need for additional retraining. This capability of effectively fine-tuning policies in simulation on novel tasks, and transferring these policies to the real world in zero-shot, highlights the potential for deploying high-performance solutions in real-world assembly tasks.

(3) Continual Learning with Skill-Library Expansion: Rather than training numerous specialist (i.e., single-task) policies from scratch, we propose gradually expanding a small set of initial skills via retrieval and adaptation to cover a broader range of tasks. This strategy improves sample efficiency by over 80% compared to the baseline (Tang et al., 2024) and keeps consistently efficient as the skill library and target tasks evolve. SRSA provides an efficient solution for accumulating a large-scale collection of skills.

2 Related Work

Robotic Assembly Tasks Robotic assembly is a critical manufacturing process in the automotive, aerospace, electronics, and medical device industries, but *adaptive* robotic assembly (e.g., robustness

to part types, initial part poses, perceptual noise, control error, and environmental perturbations) is largely unsolved. Research on adaptive assembly has seen significant growth in recent years (Beltran-Hernandez et al., 2020; Luo et al., 2021; Narang et al., 2022; Tang et al., 2023; Zhang et al., 2023). Despite advancements in datasets and real-world benchmarks for assembling small, realistic parts (Kimble et al., 2020; 2022; Willis et al., 2022; Tian et al., 2022), the exploration of policy learning across a wide variety of parts remains relatively limited. Most recent efforts in robotic assembly have concentrated on perception (Fu et al., 2022; Wen et al., 2022) or planning (Tian et al., 2022; 2024), rather than learning policies that are robust to disturbances and noise. Additionally, the policy-learning efforts that have addressed the widest range of assemblies have typically been restricted to <30 parts (Spector & Di Castro, 2021; Spector et al., 2022; Zhao et al., 2022). The largest study, AutoMate (Tang et al., 2024), introduced a diverse dataset featuring 100 assembly tasks with simulation environments and 3D-printable parts, and explores policy learning across these tasks. However, its approach primarily focuses on learning specialist (i.e., single-task) policies *from scratch* without leveraging prior experience or knowledge from related tasks. In contrast, our goal is to solve novel assembly tasks by leveraging skills from previously-solved assembly tasks.

Retrieval-based Policy Learning Many studies have explored techniques for utilizing datasets from other tasks for pretraining, such as visual pretraining (Parisi et al., 2022; Nair et al., 2022; Xiao et al., 2022) and multi-task imitation learning (Jang et al., 2022; Ebert et al., 2021; Shridhar et al., 2022). Recently, in robotic manipulation, some works have investigated how to incorporate offline data from other tasks during policy learning, i.e., retrieving prior data according to expert demonstrations on the target task (Nasiriany et al., 2022; Belkhale et al., 2024; Shao et al., 2021; Zha et al., 2024). For instance, Du et al. (2023) selects pertinent state-action pairs based on visual and action similarity from offline, unlabeled datasets and jointly trains a policy using a small amount of expert demonstrations and the queried data via imitation learning. Lin et al. (2024), on the other hand, emphasizes motion similarity rather than semantic similarity by retrieving state-action pairs based on optical flow representations, followed by few-shot imitation learning with expert demonstrations and the retrieved data. Kuang et al. (2024) takes a different approach by extracting a unified affordance representation from diverse data sources and hierarchically retrieving and transferring 2D affordance information based on language instructions to perform zero-shot robotic manipulation. These works primarily study *data retrieval* for general pick-and-place manipulation tasks. (Zhu et al., 2024) instead introduce a policy retriever to access relevant strategies from an external policy memory bank and a policy generator to assimilate these strategies to formulate effective responses to pick-and-place tasks. In contrast to these works, we focus on challenging contact-rich manipulation tasks, specifically investigating *policy retrieval* for such environments.

Embedding Learning for Task and Skills *Task* embedding learning has been extensively explored in meta-reinforcement learning and multi-task reinforcement learning problems, where shared knowledge across tasks can significantly enhance learning efficiency for new tasks. Most previous approaches focus on capturing task features related to visual appearance in 2D images or dynamics in transitions (James et al., 2018; Rakelly et al., 2019; Lee et al., 2020). Contrastive learning is often employed to bring similar tasks closer together in the embedding space while pushing dissimilar tasks farther apart (James et al., 2018). *Skill* embedding learning, on the other hand, leverages unstructured prior experiences (i.e., temporally extended actions that encapsulate useful behaviors) and repurposes them to solve downstream tasks. Existing methods typically train a high-level policy where the action space consists of the extracted skills (Pertsch et al., 2021; Nasiriany et al., 2022; Hausman et al., 2018; Sharma et al., 2019; Lynch et al., 2020). Although most previous approaches use skills to solve subtasks and combine sequences of skills for long-horizon tasks, we focus on selecting and adapting a single relevant skill for a new task, which is typically short-horizon but challenging to train due to exploration challenges and precise control requirements. Additionally, we integrate multiple embedding-learning approaches by *jointly* capturing three fundamental components of assembly tasks: part geometry, interaction dynamics, and expert actions. We consolidate these perspectives for more robust task representation.

3 Problem Setup

In this work, we consider the problem setting of solving a new target task leveraging pre-existing skills from a skill library. This library contains policies, each designed to solve a specific previously-encountered task. Our approach is motivated by situations where an agent can draw on knowledge

from previously-learned policies to adapt quickly to a new task at hand (Rusu et al., 2016; Tirinzoni et al., 2019; Huang et al., 2021).

Similar to the multi-task reinforcement learning (RL) formulation (Borsa et al., 2016; Sodhani et al., 2021; Calandriello et al., 2014), we consider a task space $\mathcal{T}$ where each task $T \in \mathcal{T}$ is defined as a Markov decision process (MDP) $(\mathcal{S}, \mathcal{A}, p, r, \gamma, \rho)$. In this formulation, $\mathcal{S}$ represents the state space, $\mathcal{A}$ the action space, $p(s_{t+1}|s_t, a_t)$ the transition dynamics, $r(s_t, a_t)$ the reward function, $\gamma \in [0, 1)$ the discount factor, and ρ the initial state distribution.

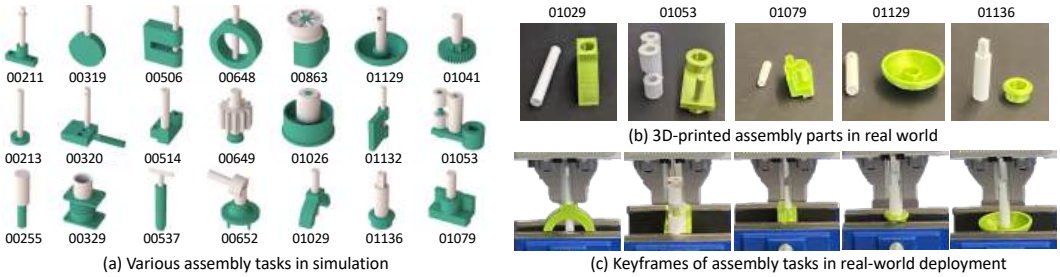

Figure 2: **Illustration of assembly tasks in AutoMate and SRSA**. (a) Samples of assembly tasks in the AutoMate benchmark. (b) 3D-printed parts of corresponding real-world assembly tasks in SRSA. (c) Keyframes from video recordings of our real-world deployments of performant policies.

Our study focuses on two-part assembly tasks, as depicted in Fig. 2. Following the setup of AutoMate (Tang et al., 2024), each environment includes a Franka robot, a *plug* (i.e., a part to be inserted), and a *socket* (i.e., the part that mates with the given plug). In the initial state, we randomize the robot configuration and socket pose, as well as the position of the plug within the robot's gripper. The goal of each task is to insert a unique plug into its corresponding socket (see Appendix A.1 for details).

The state space $\mathcal{S}$ consists of the robot arm's joint angles and velocities, the end-effector pose and its linear/angular velocities, the current plug pose, and the end-effector goal pose. The action space $\mathcal{A}$ consists of incremental pose targets for a task-space impedance controller. As described in (Tang et al., 2024), although assembly trajectories are infeasible to procedurally generate, *disassembly paths* can be easily generated, serving as reverse demonstrations that can be used by a reinforcement learning (RL) agent. Specifically, the RL reward function is composed of terms that penalize the distance to the goal, penalize simulation error, reward task difficulty in a curriculum, and imitate the reversed disassembly paths. The assembly tasks all share the same state space $\mathcal{S}$ and action space $\mathcal{A}$, but vary in part geometries, transition dynamics p, and initial state distribution ρ.

Given a target task $T \in \mathcal{T}$, we assume access to a prior task set $\mathcal{T}_{prior} = \{T_1, T_2, \cdots, T_n\} \subseteq \mathcal{T}$. With policy space $\Pi : \mathcal{S} \to \mathcal{A}$, the *skill library* contains policies $\Pi_{prior} = \{\pi_1, \pi_2, \cdots, \pi_n\} \subseteq \Pi$ that solve each of the prior tasks, respectively. To solve a target task, the goal of RL is to find a policy $\pi(a_t|s_t)$ that produces an action for each state to maximize the expected return. We propose to first retrieve a skill (i.e., policy) for the most relevant prior task (Sec. 4.1), and then rapidly and effectively adapt to the target task by fine-tuning the retrieved skill (Sec. 4.2).

4 Method

4.1 Skill Retrieval

To effectively retrieve skills from Π_{prior} that are useful for a new target task T, we require a means to measure the potential of applying a source policy $\pi_{src} \in \Pi_{prior}$ to task T. Concretely, we aim to obtain a function $F : \Pi \times \mathcal{T} \to \mathbb{R}$, which takes as input a source policy and a target task and produces a scalar score measuring how well the source policy can be adapted to the target task.

According to the simulation lemma in RL theory (Agarwal et al., 2019), the difference in expected value when applying the same policy to different tasks primarily depends on their difference in transition dynamics and initial state distributions. If we execute a source policy π_{src} on both the source task T_{src} and the target task T_{trg}, the success rates $r_{src,src}$ and $r_{src,trg}$ (on T_{src} and T_{trg}, respectively) reflect the expected value. Notably, similar success rates on these tasks indicate that their transition dynamics functions and initial state distributions might also be similar. Here, our success

rate on the source task $r_{src,src}$ will naturally be high, because the source policy π_{src} is already an expert policy on T_{src}. Thus, when the zero-shot transfer success rate $r_{src,trg}$ (i.e., applying π_{src} directly to T_{trg}) is also high (e.g., similar to $r_{src,src}$), it suggests that the two tasks might be closely aligned in terms of their dynamics. Details are in Appendix A.2.

We then hypothesize that fine-tuning a source policy on a target task with similar dynamics will be efficient, because it only requires adaptation to the small difference in dynamics. Therefore, we propose using zero-shot transfer success as a metric to gauge the potential of efficiently adapting a source policy on a target task. To identify a source policy with high zero-shot transfer success on a given target task, we propose to learn a function F to predict the zero-shot transfer success for any pair of source policy π_{src} and target task T_{trg}. The prediction $F(\pi_{src}, T_{trg})$ serves as an indicator of whether π_{src} is a strong candidate to initiate fine-tuning for the target task T_{trg}. Below, we describe the featurization of the source policies and target tasks in Sec. 4.1.1 and explain the approach to transfer success prediction with input features in Sec. 4.1.2.

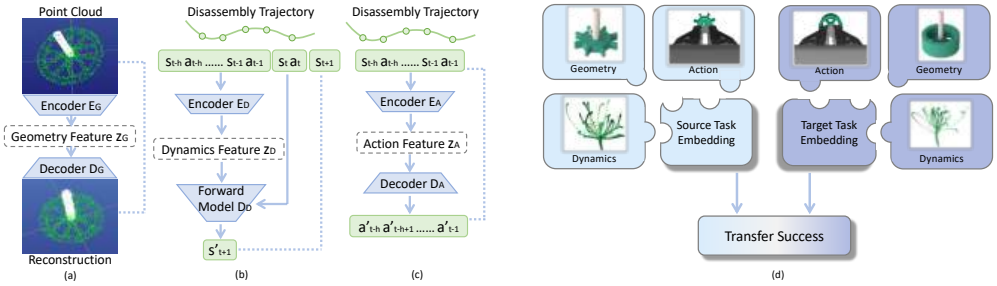

Figure 3: **Illustration of our skill retrieval approach.** We decompose the skill retrieval into task feature learning (abc) and transfer success prediction (d). (a) Geometry features are learned from point-cloud input using a PointNet autoencoder. (b) Dynamics features are learned from transition segments using a state-prediction objective. (c) Expert-action features are learned from transition segments using an action-prediction objective. (d) The zero-shot transfer success rate (of applying a source policy to a target task) is predicted using task features from source and target tasks.

4.1.1 Learning Task Features

In order to train the prediction function F, we construct a dataset of tuples $(\pi_{src}, T_{trg}, r_{src,trg})$, where $r_{src,trg}$ denotes the success rate for zero-shot transfer of a source policy π_{src} when applied to a target task T_{trg}. However, due to the limited number of (π_{src}, T_{trg}) pairs (specifically, during training, we have $n \times n$ pairs for a total of n tasks in $\mathcal{T}_{prior}$), we need a strong featurization of both the source policy and target task for efficient learning of F.

The source policy π_{src} is an expert policy for the corresponding source task T_{src}, and there is a one-to-one mapping between policies and tasks in the skill library. Thus, we can utilize the features of the source task to represent the source policy. For assembly tasks, each task differs along three fundamental axes: part geometry, interaction dynamics, and expert actions that solve the task. Thus, we propose a framework that jointly captures features of geometry, dynamics, and expert actions to represent the tasks, allowing us to efficiently learn the transfer success predictor F (Fig. 3).

When learning geometry features, we assume access to object meshes for both seen and novel tasks; this assumption is well-grounded in industry, where CAD models are widely available, allowing us to learn embeddings of 3D geometry. However, learning features for dynamics and expert actions poses a unique challenge. For new assembly tasks, we assume that expert demonstrations are *not* available, as these are typically tedious to obtain and often suboptimal for assembly tasks. This deficit prevents us from easily computing dynamics or action embeddings.

We draw insight from (Tian et al., 2022; Tang et al., 2024), which noted that, while procedurally generating assembly demonstrations for new tasks is intractable (narrow-passage problem), *disassembly paths* can be trivially generated by employing a compliant low-level controller to lift an inserted plug from its socket and move it to a randomized pose. We propose learning features for dynamics and expert actions by using these *disassembly paths* and hypothesize that such features are useful for predicting transfer success for assembly; we later empirically support this hypothesis.

Using the parts' point clouds or transition sequences from disassembly, we learn encoders E_G, E_D, and E_A to capture features z_G (representing geometry), z_D (representing forward dynamics), and z_A (representing expert actions). We also train decoders D_G, D_D, and D_A conditioned on these features to predict point cloud for geometry, next state for dynamics, and action sequence for expert action choices. In Appendix A.4, we explain the implementation details for learning these features.

4.1.2 Predicting Transfer Success

We consolidate task features to develop the transfer success prediction function F. During training, we formulate any two tasks from the prior task set $\mathcal{T}_{prior}$ as a source-target task pair. For each pair (π_{src}, T_{trg}), we evaluate the source policy π_{src} on the target task T_{trg} to obtain the zero-shot transfer success rate $r_{src,trg}$. This process enables us to collect a training dataset of tuples $(\pi_{src}, T_{trg}, r_{src,trg})$ from the prior skill library. As explained in Sec. 4.1.1, we feed the point cloud and transition segments into encoders. The features of geometry, dynamics, and expert action are concatenated together to get task features z_{src} and z_{trg}. Then the concatenated task features go through an MLP to predict the transfer success $r_{src,trg}$, as illustrated in Fig. 3(d). Formally, we train the function F to minimize the objective function (Eq. 1):

$$\begin{aligned}\mathcal{L} &= \|F(\pi_{src}, T_{trg}) - r_{src,trg}\|^2 = \|MLP(z_{src}, z_{trg}) - r_{src,trg}\|^2 \\ &= \|MLP(E_G(P_{src}), E_D(\tau_{src}), E_A(\tau_{src}), E_G(P_{trg}), E_D(\tau_{trg}), E_A(\tau_{trg})) - r_{src,trg}\|^2 \end{aligned} \quad (1)$$

At test time, we use the function F to predict the transfer success of applying any prior policy to a new task T_{trg} as $F(\pi_{src}, T_{trg})$. For inputs to the function F, we sample the point clouds $P_1, P_2, \cdots, P_m$ from parts' meshes and transition segments $\tau_1, \tau_2, \cdots, \tau_m$ from disassembly trajectories. We compute the averaged prediction for these samples, i.e. $F(\pi_{src},T_{trg})=\frac{1}{m}\sum_{i=1}^{m} MLP(E_G(P_{src,i}),E_D(\tau_{src,i}),E_A(\tau_{src,i}),E_G(P_{trg,i}),E_D(\tau_{trg,i}),E_A(\tau_{trg,i}))$. In this manner, we infer the predicted transfer success $F(\pi_{src}, T_{trg})$ for all source policies π_{src} in the prior skill library $\Pi_{prior} = \{\pi_1, \pi_2, \cdots, \pi_n\}$. Our retrieved policy is the source policy with the highest predicted transfer success, defined as $\arg\max_{\pi_{src}} F(\pi_{src}, T_{trg})$.

4.2 Skill Adaptation

As mentioned in Sec. 3, our ultimate goal is to solve the new task as an RL problem. The retrieved skill is used to initialize the policy network $\pi_\theta(a_t|s_t)$, and we subsequently use proximal policy optimization (PPO) (Schulman et al., 2017) to fine-tune the policy on the target task.

This initialization provides a strong start for policy learning, as the initial trials with the retrieved skills can achieve a reasonable success rate. Inspired by self-imitation learning (Oh et al., 2018), we fully exploit these positive experiences gained during the initial phase of fine-tuning. We maintain a replay buffer $\mathcal{D} = \{(s_t, a_t, R_t)\}$ to store the transitions encountered throughout training, where $R_t = \sum_{k=t}^{\infty} \gamma^{k-t} r_k$ is the discounted sum of rewards. We prioritize the state-action pairs (s_t, a_t) based on R_t and imitate those pairs with high rewards. The objective function is defined in Eq. 2:

$$\mathcal{L}^{sil} = \mathbb{E}_{(s,a,R)\in\mathcal{D}}[\mathcal{L}^{sil}_{policy} + \beta\mathcal{L}^{sil}_{value}] \quad (2)$$

where $\mathcal{L}^{sil}_{policy} = -\log \pi_\theta(a|s)(R - V_\theta(s))_+$, $\mathcal{L}^{sil}_{value} = \frac{1}{2}\|(R - V_\theta(s))_+\|^2$, $(\cdot)_+ = \max(\cdot, 0)$, and π_θ and V_θ are the policy and value function parameterized by θ (see details in Appendix A.3).

As training progresses, the agent collects higher rewards on the target task, leading to an expanding replay buffer filled with improved experiences. As analyzed in (Tang, 2020), this self-imitation mechanism accelerates the agent's convergence to encountered high-reward behavior, even though it may introduce some bias into the policy. In our case, the behavior derived from the retrieved skill is advantageous for the target task. We find that self-imitation learning significantly enhances and stabilizes policy fine-tuning, proving especially beneficial in sparse-reward scenarios.

4.3 Continual Learning with Skill-Library Expansion

Continual learning investigates learning various tasks in a sequential fashion. The primary objective is to overcome the forgetting of previously-learned tasks and to leverage the earlier knowledge for better performance and/or faster convergence on incoming tasks (Ring, 1994; Xu & Zhu, 2018; Abel et al., 2024). We integrate SRSA in the continual-learning setup and gradually expand

the skill library. Specifically, we begin with an initial skill library Π_{prior} corresponding to prior tasks $\mathcal{T}_{prior}$. When faced with a new batch of tasks $T^j = \{T_1, T_2, \cdots, T_k\}$, we apply SRSA to retrieve and fine-tune policies for each new task T_i. The learned policies are then incorporated as $\mathcal{T}_{prior} = \mathcal{T}_{prior} \cup \{T_i\}$; $\Pi_{prior} = \Pi_{prior} \cup \{\pi_i\}$. This approach allows us to efficiently tackle new tasks by leveraging the skill library and simultaneously prevent the forgetting of previously learned tasks by maintaining the skill library. See Appendix A.3 for the algorithm pseudocode.

5 EXPERIMENTS

We design experiments to answer the following questions: (1) Compared with baseline retrieval approaches, can SRSA retrieve source policies that achieve a better zero-shot transfer success rate on target tasks? (2) Can SRSA improve learning performance, stability, and efficiency on target tasks? (3) Can we deploy high-performing policies from simulation in zero-shot to the real-world? (4) Can SRSA be applied in the continual-learning scenario to improve learning efficiency by gradually expanding its skill library? We investigate these questions on the AutoMate benchmark, which consists of 100 two-part assembly tasks with diverse parts, enabling us to study challenging contact-rich assembly tasks in simulation and the real world.

5.1 SKILL RETRIEVAL

AutoMate provides meshes and disassembly trajectories for each task. We use these data to learn the task embedding for retrieval. We compare SRSA to the following retrieval strategies as baselines. **Signature**: retrieve the task with the closest path signature representing disassembly trajectories as a collection of path integrals (Tang et al., 2024) **Behavior**: retrieve the task with the closest VAE embedding of state-action pairs on disassembly trajectories. **Forward**: retrieve the task with closest latent vector for transition sequence τ on disassembly trajectories, where the latent vector is used to predict forward dynamics. **Geometry**: retrieve the task with closest PointNet encoding for point clouds of the assembly assets. Implementation details can be found in Appendix A.4.

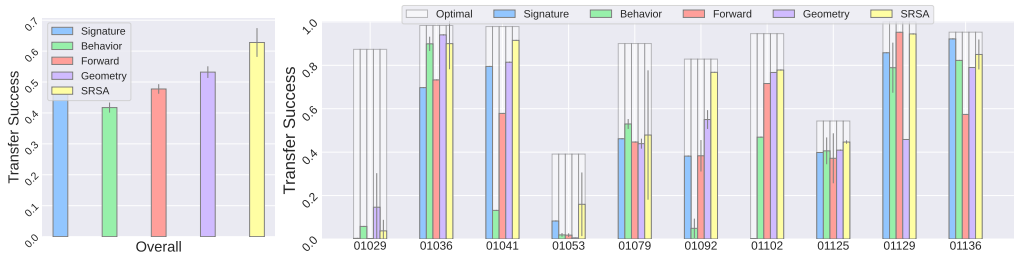

Figure 4: **Transfer success of retrieved skills when applied to test tasks**. For each test task, we retrieve a policy from the prior skill library using 5 different approaches (4 baselines and SRSA). We train each approach for 3 random seeds if it involves training neural networks. **Left**: We illustrate success rate averaged on 10 test tasks. **Right**: For each test task, we show the mean and standard deviation of transfer success over 3 seeds. Overall, SRSA substantially outperforms baselines.

Given 100 tasks in AutoMate benchmark, we split the task set to have 90 prior tasks to build the skill library and10 tasks as the new test tasks to solve. For both our and baseline methods, we train the retrieval model for three runs with different random seeds, and report the average and standard deviation of transfer success over three runs. Fig. 4 shows the result on the test task set. SRSA performs best or second-best on all test tasks, except for one very challenging assembly where all methods perform poorly (01029). In Appendix A.5, we additionally show the comparison for other choices to split prior and test task sets. Overall, SRSA retrieves source policies that obtain around 20% higher success rates on the target tasks, compared with baselines.

5.2 SKILL ADAPTATION

In this section, we investigate policy learning on test tasks given the skill library. We compare AutoMate (i.e., learning specialist policies from scratch (Tang et al., 2024)) and SRSA (i.e., fine-tuning retrieved specialist policy with self-imitation learning). Details are in Appendix A.4.

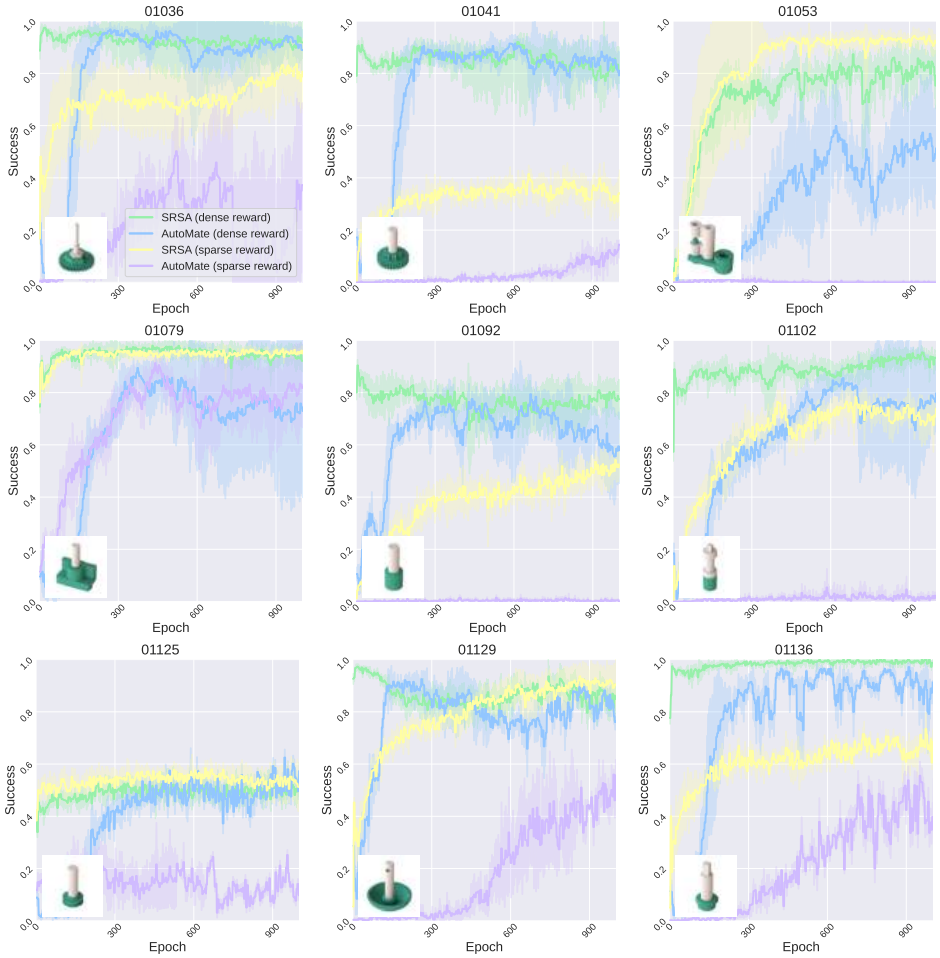

Figure 5: **Learning curves on test tasks.** The x-axis and y-axis represent training epochs (where each epoch consists of 128 environment steps over 256 parallel environments) and success rate, respectively. The solid line shows the mean success rate over 5 runs with different random seeds, and the shaded area denotes the standard deviation.

We consider both the dense-reward setting (identical to AutoMate) and the sparse-reward setting, without the use of disassembly demonstrations or a curriculum. The sparse-reward setting only provides a non-zero reward signal to the agent when the assembly task succeeds. It is designed to emulate the real-world RL fine-tuning setting, where dense-reward information can be much more challenging to acquire.

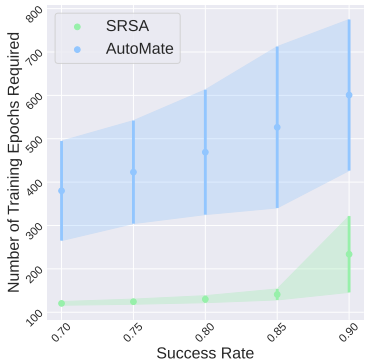

Figure 6: **Sample efficiency of policy learning on test set**. To achieve a desired success rate (here, 0.70, 0.75, 0.80, 0.85, or 0.90), we identify how many training epochs are required for each run. We illustrate the mean and standard deviation across 5 runs with the points and error bars in the figure, averaged over 10 test tasks.

Fig. 5 shows learning curves on the test task set. In the dense-reward setting, SRSA achieves strong performance with a fewer number of training epochs. In the sparse-reward setting, AutoMate struggles to achieve a reasonable success rate, whereas SRSA benefits from the retrieved skill initialization and self-imitation learning to reach higher performance. Additionally, in both settings, the learning curves of AutoMate exhibit instability with fluctuating success rates as training goes on. In Tab. 2 and Tab. 3 in Appendix A.5, we summarize the success rate at the last epoch of training. In the dense-reward setting, SRSA reaches a mean success rate of 84.7% better than AutoMate (69.4%), corresponding to a relative improvement of 22% in performance with a substantially smaller standard deviation, i.e. 3.7x greater stability. In the sparse-reward setting, SRSA delivers a remarkable 139% relative improvement in average success rate compared to the baseline. Fig. 6

demonstrates the number of training epochs required to reach a desired success rate in the dense-reward setting. Averaged over 10 test tasks, SRSA requires far fewer training samples, i.e., at least 2.4 times fewer training epochs, to achieve an arbitrary success threshold.

5.3 Real-World Deployment

We now deploy the trained specialist policies in the real world. As in (Tang et al., 2024), we place the robot in lead-through (a.k.a., manual guide mode), grasp a plug, guide it into the socket, and record the pose as a target pose. We then programmatically lift the plug until free from contact, apply a perturbation for the position and rotation of the end effector, and deploy a policy to assembly the plug into the socket. Such conditions emulate the control error and perceptual noise that are experienced in full assembly pipelines. In Tab. 7, we record the performance of the best checkpoint over 500 training epochs. In this relatively-brief training time, SRSA reaches higher success rates than the baseline for real-world assembly tasks. We show keyframes of real-world assembly tasks in Fig. 2(c). For videos of the policy execution, please refer to the project website `https://srsa2024.github.io/`.

Asset ID	01029	01053	01079	01129	01136	Overall
AutoMate	7/10	1/10	7/10	4/10	8/10	54%
SRSA	9/10	8/10	8/10	10/10	10/10	90%

Figure 7: **Real-world evaluation.** We take the best checkpoint of policies across 5 runs within 500 epochs and report the success rate over 10 trials for each task.

5.4 Continual Learning

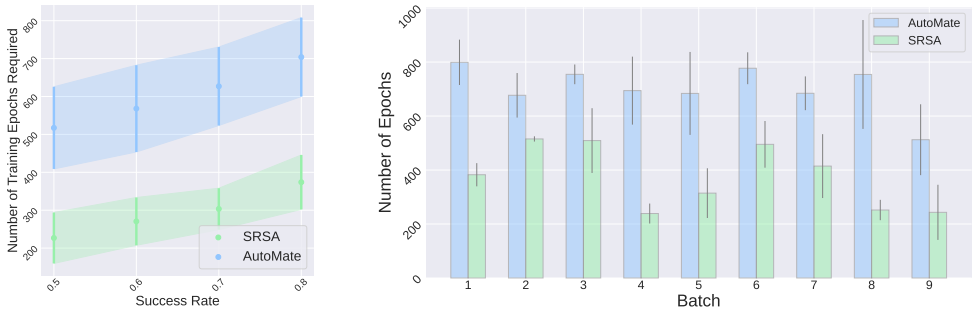

(a) (b)

Figure 8: **(a) Sample efficiency of continual policy learning.**. We report the number of training epochs required to reach desired success rates (0.5, 0.6, 0.7, 0.8). We calculate the mean and standard deviation of required training epochs over 5 runs, and report the average over 90 tasks. **(b) Number of training epochs required in continual learning.** We sequentially introduce 9 batches of new tasks for policy learning, with each batch containing 10 new tasks. For each batch, we show the mean and standard deviation of training epochs required to reach a success rate of 0.8. Obviously, SRSA requires less number of training epochs to reach a good success rate.

We study the continual-learning setting to obtain policies for each of the 100 AutoMate tasks. Rather than training 100 policies from scratch in parallel, we start from a skill library with 10 tasks, and train 10 new policies for 10 new tasks utilizing the skill library. We repeat this process for 9 iterations, eventually covering the entire benchmark. Essentially, we have a skill library that is gradually expanded with an increasing number of specialist policies.

In Fig. 8, we compare the sample efficiency of SRSA and AutoMate when learning specialist policies for 90 tasks outside the initial skill library. We consider different desired success rates, and report the number of training epochs required to reach each success rate. Overall, SRSA requires fewer training epochs to reach the desired success rate, demonstrating an 84% relative improvement in sample efficiency (Fig. 8(a)). For each batch of new tasks, SRSA is more efficient than the baseline regardless of the skill library and target tasks (Fig. 8(b)). In Fig. 14 in Appendix, we show the success rates for the highest-reward checkpoints encountered in 5 runs for each task. SRSA achieves an average success rate of 79% compared to AutoMate's 70% across 100 tasks, while also exhibiting better training efficiency. In Appendix A.5, we present learning results for another ordering of batches of tasks, showing that the advantage of SRSA is agnostic to the order of encountering new tasks.

6 ABLATION STUDY

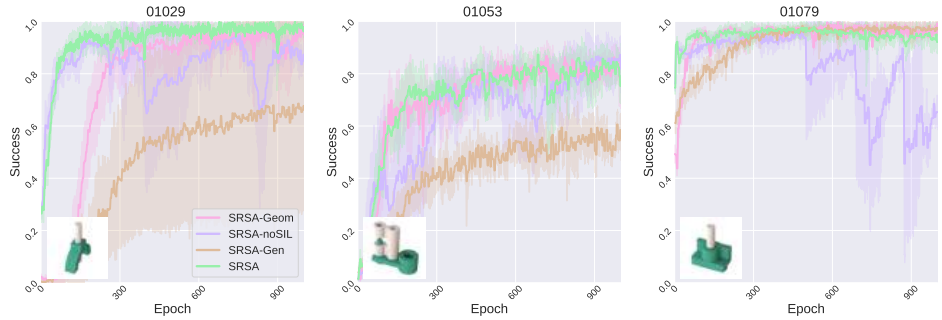

Figure 9: **Comparison for variants of SRSA with different changing component**. For each method, we have 5 runs with different random seeds. The learning curves show mean and standard deviation of success rate over these runs. We show learning curves for more tasks in Appendix A.5.

Effect of Skill Retrieval In order to verify the effect of skill retrieval, we conduct skill adaptation with retrieved skills using only a geometry embedding, i.e., the second best skill-retrieval approach evaluated in Fig. 3. Fig. 9 shows the performance of policy fine-tuning for both our skill retrieval approach (SRSA) and the geometry-based skill retrieval (SRSA-Geom). One can observe that retrieving a worse skill hinders learning efficiency, which starts from a lower success rate and requires more training epochs to reach high performance. This shows that our retrieval approach with better zero-shot transfer success also improves adaptation efficiency.

Effect of Self-imitation Learning To demonstrate the benefits of self-imitation learning (SIL) in policy fine-tuning, we compare SRSA to the variant without this component (SRSA-noSIL). In Fig. 9, SRSA outperforms the variant in terms of learning stability. In particular, SRSA-noSIL suffers from more fluctuations during fine-tuning and a larger standard deviation of success rate (shaded area) across runs with different seeds.

Effect of Generalist Policy We analyze whether fine-tuning a generalist policy outperforms fine-tuning a selected specialist policy. For policy initialization, we use the generalist policy for 20 training tasks from (Tang et al., 2024) Although it does not cover numerous tasks, it is the strongest generalist policy reported to date that can solve a diverse set of assembly tasks with an $> 80\%$ success rate (Tang et al., 2024). Fig. 9 shows the learning curves of fine-tuning the generalist policy on unseen tasks (SRSA-Gen). We observe that SRSA-Gen provides a weaker initialization compared to SRSA. This may be because the generalist policy's knowledge from the training tasks is less specialized than the skills retrieved by SRSA. Also, the adaptation is less efficient, possibly due to the larger neural network in generalist policy, which requires more fine-tuning to adapt to new tasks.

7 CONCLUSION

In this paper, we propose a pipeline to retrieve and adapt specialist policies to solve new assembly tasks. To learn a retrieval model, we jointly learn features from geometry, dynamics and expert actions to represent tasks, and predict transfer success to implicitly capture other transfer-related factors from tasks. By combining skill retrieval with policy fine-tuning and self-imitation learning, our method efficiently learns simulation-based policies. We demonstrate that these policies are transferable to real-world robots for assembly tasks. Additionally, we demonstrate that our approach can be used to continuously expand a skill library through efficient learning of various skills.

Our work has three key limitations: First, although we train policies for all assembly tasks in a leading benchmark (Tang et al., 2024), we do not address assemblies requiring rotational or helical motion (e.g., nut-and-bolt assembly). Second, we primarily concentrate on learning specialist (i.e., single-task) policies; future work could explore training generalist (i.e., multi-task) policies, and furthermore, incorporating knowledge from both specialist and generalist policies to solve novel tasks with even greater efficiency. Third, although our real-world success rates outperform the state-of-the-art in sim-to-real transfer for our examined tasks, they still fall short of 95+% success rates required for industry-level deployment. We believe that RL fine-tuning directly in real-world settings could help bridge the sim-to-real gap and further improve success rates.

REFERENCES

David Abel, André Barreto, Benjamin Van Roy, Doina Precup, Hado P van Hasselt, and Satinder Singh. A definition of continual reinforcement learning. *Advances in Neural Information Processing Systems*, 36, 2024.

Alekh Agarwal, Nan Jiang, Sham M Kakade, and Wen Sun. Reinforcement learning: Theory and algorithms. *CS Dept., UW Seattle, Seattle, WA, USA, Tech. Rep*, 32:96, 2019.

Suneel Belkhale, Tianli Ding, Ted Xiao, Pierre Sermanet, Quon Vuong, Jonathan Tompson, Yevgen Chebotar, Debidatta Dwibedi, and Dorsa Sadigh. Rt-h: Action hierarchies using language. *arXiv preprint arXiv:2403.01823*, 2024.

Cristian C. Beltran-Hernandez, Damien Petit, Ixchel G. Ramirez-Alpizar, and Kensuke Harada. Variable compliance control for robotic peg-in-hole assembly: A deep-reinforcement-learning approach. *Applied Sciences*, 2020.

Diana Borsa, Thore Graepel, and John Shawe-Taylor. Learning shared representations in multi-task reinforcement learning. *arXiv preprint arXiv:1603.02041*, 2016.

Daniele Calandriello, Alessandro Lazaric, and Marcello Restelli. Sparse multi-task reinforcement learning. *Advances in neural information processing systems*, 27, 2014.

Maximilian Du, Suraj Nair, Dorsa Sadigh, and Chelsea Finn. Behavior retrieval: Few-shot imitation learning by querying unlabeled datasets. *arXiv preprint arXiv:2304.08742*, 2023.

Frederik Ebert, Yanlai Yang, Karl Schmeckpeper, Bernadette Bucher, Georgios Georgakis, Kostas Daniilidis, Chelsea Finn, and Sergey Levine. Bridge data: Boosting generalization of robotic skills with cross-domain datasets. *arXiv preprint arXiv:2109.13396*, 2021.

Bowen Fu, Sek Kun Leong, Xiaocong Lian, and Xiangyang Ji. 6d robotic assembly based on rgb-only object pose estimation. In *2022 IEEE/RSJ International Conference on Intelligent Robots and Systems (IROS)*, pp. 4736–4742. IEEE, 2022.

Ankit Goyal, Valts Blukis, Jie Xu, Yijie Guo, Yu-Wei Chao, and Dieter Fox. Rvt-2: Learning precise manipulation from few demonstrations. *arXiv preprint arXiv:2406.08545*, 2024.

Yijie Guo, Qiucheng Wu, and Honglak Lee. Learning action translator for meta reinforcement learning on sparse-reward tasks. In *Proceedings of the AAAI Conference on Artificial Intelligence*, volume 36, pp. 6792–6800, 2022.

Karol Hausman, Jost Tobias Springenberg, Ziyu Wang, Nicolas Heess, and Martin Riedmiller. Learning an embedding space for transferable robot skills. In *International Conference on Learning Representations*, 2018.

Biwei Huang, Fan Feng, Chaochao Lu, Sara Magliacane, and Kun Zhang. Adarl: What, where, and how to adapt in transfer reinforcement learning. *arXiv preprint arXiv:2107.02729*, 2021.

Stephen James, Michael Bloesch, and Andrew J Davison. Task-embedded control networks for few-shot imitation learning. In *Conference on robot learning*, pp. 783–795. PMLR, 2018.

Eric Jang, Alex Irpan, Mohi Khansari, Daniel Kappler, Frederik Ebert, Corey Lynch, Sergey Levine, and Chelsea Finn. Bc-z: Zero-shot task generalization with robotic imitation learning. In *Conference on Robot Learning*, pp. 991–1002. PMLR, 2022.

Kenneth Kimble, Karl Van Wyk, Joe Falco, Elena Messina, Yu Sun, Mizuho Shibata, Wataru Uemura, and Yasuyoshi Yokokohji. Benchmarking protocols for evaluating small parts robotic assembly systems. *IEEE robotics and automation letters*, 5(2):883–889, 2020.

Kenneth Kimble, Justin Albrecht, Megan Zimmerman, and Joe Falco. Performance measures to benchmark the grasping, manipulation, and assembly of deformable objects typical to manufacturing applications. *Frontiers in Robotics and AI*, 9:999348, 2022.

Yuxuan Kuang, Junjie Ye, Haoran Geng, Jiageng Mao, Congyue Deng, Leonidas Guibas, He Wang, and Yue Wang. Ram: Retrieval-based affordance transfer for generalizable zero-shot robotic manipulation. *arXiv preprint arXiv:2407.04689*, 2024.

Kimin Lee, Younggyo Seo, Seunghyun Lee, Honglak Lee, and Jinwoo Shin. Context-aware dynamics model for generalization in model-based reinforcement learning. In *International Conference on Machine Learning*, pp. 5757–5766. PMLR, 2020.

Li-Heng Lin, Yuchen Cui, Amber Xie, Tianyu Hua, and Dorsa Sadigh. Flowretrieval: Flow-guided data retrieval for few-shot imitation learning. *arXiv preprint arXiv:2408.16944*, 2024.

Jianlan Luo, Oleg Sushkov, Rugile Pevceviciute, Wenzhao Lian, Chang Su, Mel Vecerik, Ning Ye, Stefan Schaal, and Jon Scholz. Robust multi-modal policies for industrial assembly via reinforcement learning and demonstrations: A large-scale study. *arXiv preprint arXiv:2103.11512*, 2021.

Corey Lynch, Mohi Khansari, Ted Xiao, Vikash Kumar, Jonathan Tompson, Sergey Levine, and Pierre Sermanet. Learning latent plans from play. In *Conference on robot learning*, pp. 1113–1132. PMLR, 2020.

Tongzhou Mu, Zhan Ling, Fanbo Xiang, Derek Yang, Xuanlin Li, Stone Tao, Zhiao Huang, Zhiwei Jia, and Hao Su. Maniskill: Generalizable manipulation skill benchmark with large-scale demonstrations. *arXiv preprint arXiv:2107.14483*, 2021.

Suraj Nair, Aravind Rajeswaran, Vikash Kumar, Chelsea Finn, and Abhinav Gupta. R3m: A universal visual representation for robot manipulation. *arXiv preprint arXiv:2203.12601*, 2022.

Yashraj Narang, Kier Storey, Iretiayo Akinola, Miles Macklin, Philipp Reist, Lukasz Wawrzyniak, Yunrong Guo, Adam Moravanszky, Gavriel State, Michelle Lu, et al. Factory: Fast contact for robotic assembly. *arXiv preprint arXiv:2205.03532*, 2022.

Soroush Nasiriany, Tian Gao, Ajay Mandlekar, and Yuke Zhu. Learning and retrieval from prior data for skill-based imitation learning. *arXiv preprint arXiv:2210.11435*, 2022.

Junhyuk Oh, Yijie Guo, Satinder Singh, and Honglak Lee. Self-imitation learning. In *International conference on machine learning*, pp. 3878–3887. PMLR, 2018.

Simone Parisi, Aravind Rajeswaran, Senthil Purushwalkam, and Abhinav Gupta. The unsurprising effectiveness of pre-trained vision models for control. In *international conference on machine learning*, pp. 17359–17371. PMLR, 2022.

Karl Pertsch, Youngwoon Lee, and Joseph Lim. Accelerating reinforcement learning with learned skill priors. In *Conference on robot learning*, pp. 188–204. PMLR, 2021.

Charles R Qi, Hao Su, Kaichun Mo, and Leonidas J Guibas. Pointnet: Deep learning on point sets for 3d classification and segmentation. In *Proceedings of the IEEE conference on computer vision and pattern recognition*, pp. 652–660, 2017.

Kate Rakelly, Aurick Zhou, Chelsea Finn, Sergey Levine, and Deirdre Quillen. Efficient off-policy meta-reinforcement learning via probabilistic context variables. In *International conference on machine learning*, pp. 5331–5340. PMLR, 2019.

Mark Bishop Ring. *Continual learning in reinforcement environments*. The University of Texas at Austin, 1994.

Andrei A Rusu, Neil C Rabinowitz, Guillaume Desjardins, Hubert Soyer, James Kirkpatrick, Koray Kavukcuoglu, Razvan Pascanu, and Raia Hadsell. Progressive neural networks. *arXiv preprint arXiv:1606.04671*, 2016.

John Schulman, Filip Wolski, Prafulla Dhariwal, Alec Radford, and Oleg Klimov. Proximal policy optimization algorithms. *arXiv preprint arXiv:1707.06347*, 2017.

Lin Shao, Toki Migimatsu, Qiang Zhang, Karen Yang, and Jeannette Bohg. Concept2robot: Learning manipulation concepts from instructions and human demonstrations. *The International Journal of Robotics Research*, 40(12-14):1419–1434, 2021.

Archit Sharma, Shixiang Gu, Sergey Levine, Vikash Kumar, and Karol Hausman. Dynamics-aware unsupervised discovery of skills. *arXiv preprint arXiv:1907.01657*, 2019.

Mohit Shridhar, Lucas Manuelli, and Dieter Fox. Cliport: What and where pathways for robotic manipulation. In *Conference on robot learning*, pp. 894–906. PMLR, 2022.

Shagun Sodhani, Amy Zhang, and Joelle Pineau. Multi-task reinforcement learning with context-based representations. In *International Conference on Machine Learning*, pp. 9767–9779. PMLR, 2021.

Oren Spector and Dotan Di Castro. Insertionnet-a scalable solution for insertion. *IEEE Robotics and Automation Letters*, 6(3):5509–5516, 2021.

Oren Spector, Vladimir Tchuiev, and Dotan Di Castro. Insertionnet 2.0: Minimal contact multi-step insertion using multimodal multiview sensory input. In *2022 International Conference on Robotics and Automation (ICRA)*, pp. 6330–6336. IEEE, 2022.

Bingjie Tang, Michael A Lin, Iretiayo Akinola, Ankur Handa, Gaurav S Sukhatme, Fabio Ramos, Dieter Fox, and Yashraj Narang. Industreal: Transferring contact-rich assembly tasks from simulation to reality. *arXiv preprint arXiv:2305.17110*, 2023.

Bingjie Tang, Iretiayo Akinola, Jie Xu, Bowen Wen, Ankur Handa, Karl Van Wyk, Dieter Fox, Gaurav S Sukhatme, Fabio Ramos, and Yashraj Narang. Automate: Specialist and generalist assembly policies over diverse geometries. *arXiv preprint arXiv:2407.08028*, 2024.

Yunhao Tang. Self-imitation learning via generalized lower bound q-learning. *Advances in neural information processing systems*, 33:13964–13975, 2020.

Yunsheng Tian, Jie Xu, Yichen Li, Jieliang Luo, Shinjiro Sueda, Hui Li, Karl DD Willis, and Wojciech Matusik. Assemble them all: Physics-based planning for generalizable assembly by disassembly. *ACM Transactions on Graphics (TOG)*, 41(6):1–11, 2022.

Yunsheng Tian, Karl DD Willis, Bassel Al Omari, Jieliang Luo, Pingchuan Ma, Yichen Li, Farhad Javid, Edward Gu, Joshua Jacob, Shinjiro Sueda, et al. Asap: automated sequence planning for complex robotic assembly with physical feasibility. In *2024 IEEE International Conference on Robotics and Automation (ICRA)*, pp. 4380–4386. IEEE, 2024.

Andrea Tirinzoni, Mattia Salvini, and Marcello Restelli. Transfer of samples in policy search via multiple importance sampling. In *International Conference on Machine Learning*, pp. 6264–6274. PMLR, 2019.

Weikang Wan, Haoran Geng, Yun Liu, Zikang Shan, Yaodong Yang, Li Yi, and He Wang. Unidexgrasp++: Improving dexterous grasping policy learning via geometry-aware curriculum and iterative generalist-specialist learning. In *Proceedings of the IEEE/CVF International Conference on Computer Vision*, pp. 3891–3902, 2023.

Bowen Wen, Wenzhao Lian, Kostas Bekris, and Stefan Schaal. You only demonstrate once: Category-level manipulation from single visual demonstration. *arXiv preprint arXiv:2201.12716*, 2022.

Karl DD Willis, Pradeep Kumar Jayaraman, Hang Chu, Yunsheng Tian, Yifei Li, Daniele Grandi, Aditya Sanghi, Linh Tran, Joseph G Lambourne, Armando Solar-Lezama, et al. Joinable: Learning bottom-up assembly of parametric cad joints. In *Proceedings of the IEEE/CVF conference on computer vision and pattern recognition*, pp. 15849–15860, 2022.

Tete Xiao, Ilija Radosavovic, Trevor Darrell, and Jitendra Malik. Masked visual pre-training for motor control. *arXiv preprint arXiv:2203.06173*, 2022.

Ju Xu and Zhanxing Zhu. Reinforced continual learning. *Advances in neural information processing systems*, 31, 2018.

Lihan Zha, Yuchen Cui, Li-Heng Lin, Minae Kwon, Montserrat Gonzalez Arenas, Andy Zeng, Fei Xia, and Dorsa Sadigh. Distilling and retrieving generalizable knowledge for robot manipulation via language corrections. In *2024 IEEE International Conference on Robotics and Automation (ICRA)*, pp. 15172–15179. IEEE, 2024.

Xiang Zhang, Changhao Wang, Lingfeng Sun, Zheng Wu, Xinghao Zhu, and Masayoshi Tomizuka. Efficient sim-to-real transfer of contact-rich manipulation skills with online admittance residual learning. In *Conference on Robot Learning*, pp. 1621–1639. PMLR, 2023.

Tony Z Zhao, Jianlan Luo, Oleg Sushkov, Rugile Pevceviciute, Nicolas Heess, Jon Scholz, Stefan Schaal, and Sergey Levine. Offline meta-reinforcement learning for industrial insertion. In *2022 international conference on robotics and automation (ICRA)*, pp. 6386–6393. IEEE, 2022.

Yichen Zhu, Zhicai Ou, Xiaofeng Mou, and Jian Tang. Retrieval-augmented embodied agents. In *Proceedings of the IEEE/CVF Conference on Computer Vision and Pattern Recognition*, pp. 17985–17995, 2024.

A APPENDIX

A.1 ROBOT SETUP

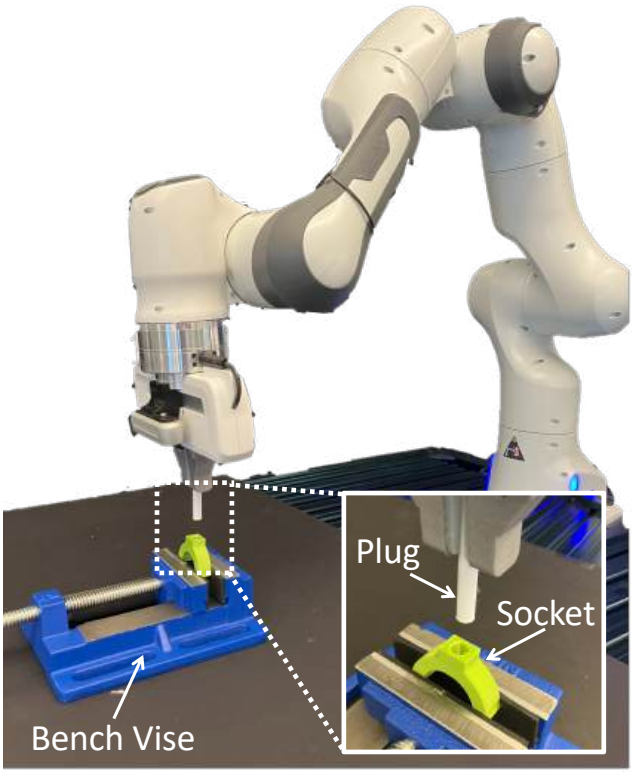

Figure 10: **Real-world experimental setup**. A Franka Panda robot and a bench vise are mounted to a tabletop. At the beginning of each episode, a 3D-printed plug is grasped by the robot gripper and and a 3D-printed socket is haphazardly placed in the bench vise. The task is to control the robot arm and fully insert the plug into the socket.

A.2 MOTIVATION WITH THEORETICAL PERSPECTIVE

Transferring knowledge from a source task to a target task can improve training efficiency and asymptotic performance. Consider a source task T_j and target task T_i, which are MDPs that share state space $\mathcal{S}$, action space $\mathcal{A}$, and reward function r, but have distinct transition functions p_i, p_j and initial state distributions ρ_i, ρ_j. To measure the transferability of a policy, we apply the same policy on both tasks and examine the difference in their expected values. Here we note that the value difference depends primarily on the difference in their transition functions p_i, p_j and initial state distributions ρ_i, ρ_j (Proposition 1).

Proposition 1. *Let $T_i = \{\mathcal{S}, \mathcal{A}, p_i, r, \gamma, \rho_i\}$ and $T_j = \{\mathcal{S}, \mathcal{A}, p_j, r, \gamma, \rho_j\}$ be two MDPs in the task space $\mathcal{T}$. Applying a policy π on T_i and T_j, we have a function f to describe the value difference:*

$$V^{\pi}(\rho_i, T_i) - V^{\pi}(\rho_j, T_j) = f(p_i - p_j, \rho_i - \rho_j)$$

Proof.

$$
\begin{aligned}
V^\pi(\rho_i, T_i) - V^\pi(\rho_j, T_j) &= \mathbb{E}_{s\sim\rho_i(\cdot)}\mathbb{E}_{a\sim\pi(\cdot|s)}Q^\pi(s,a,T_i) - \mathbb{E}_{s\sim\rho_j(\cdot)}\mathbb{E}_{a\sim\pi(\cdot|s)}Q^\pi(s,a,T_j) \\
&= \mathbb{E}_{s\sim\rho_i(\cdot)}\mathbb{E}_{a\sim\pi(\cdot|s)}[Q^\pi(s,a,T_i) - Q^\pi(s,a,T_j)] \\
&\quad + \mathbb{E}_{s\sim\rho_i(\cdot)}\mathbb{E}_{a\sim\pi(\cdot|s)}Q^\pi(s,a,T_j) - \mathbb{E}_{s\sim\rho_j(\cdot)}\mathbb{E}_{a\sim\pi(\cdot|s)}Q^\pi(s,a,T_j) \\
&= \mathbb{E}_{s\sim\rho_i(\cdot)}\mathbb{E}_{a\sim\pi(\cdot|s)}[Q^\pi(s,a,T_i) - Q^\pi(s,a,T_j)] \\
&\quad + \mathbb{E}_{s\sim\rho_i(\cdot)}V^\pi(s,T_j) - \mathbb{E}_{s\sim\rho_j(\cdot)}V^\pi(s,T_j) \\
&= \mathbb{E}_{s\sim\rho_i(\cdot)}\mathbb{E}_{a\sim\pi(\cdot|s)}[Q^\pi(s,a,T_i) - Q^\pi(s,a,T_j)] + \sum_s(\rho_i - \rho_j)V^\pi(s,T_j)
\end{aligned}
$$

For the Q-value difference $Q^\pi(s,a,T_i) - Q^\pi(s,a,T_j)$, we refer to the simulation lemma in (Agarwal et al., 2019):

$$
Q^\pi(T_i) - Q^\pi(T_j) = \gamma(I - \gamma P^\pi(T_j))^{-1}(p_i - p_j)V^\pi(T_i)
$$

where $P^\pi(T_j)$ denotes the transition matrix on state-action pairs induced by the policy π on the task T_j, i.e., $P^\pi_{(s,a),(s',a')}(T_j) = p_j(s'|s,a)\pi(a'|s')$.

Consequently, $Q^\pi(s,a,T_i) - Q^\pi(s,a,T_j)$ is the (s,a) item in the matrix $Q^\pi(T_i) - Q^\pi(T_j)$, and $Q^\pi(s,a,T_i) - Q^\pi(s,a,T_j)$ can be expressed as a function of $(p_i - p_j)$.

Overall, the value difference $V^\pi(\rho_i, T_i) - V^\pi(\rho_j, T_j)$ depends primarily on $(p_i - p_j)$ and $(\rho_i - \rho_j)$. □

Assume the reward function r is a sparse, binary term indicating task success at the end of an episode. The success rate of applying a policy π to a task T can be represented as $V^\pi(\rho) = \mathbb{E}_{s_0\sim\rho}\mathbb{E}_{\tau\sim p^\pi(\tau|s=s_0)}[\sum_{t=0}^\infty \gamma^t r_t]$. Here, our success rate $V^\pi(\rho_j, T_j)$ will naturally be high, because the source policy π is already an expert policy for the source task T_j. When the success rate of applying the source policy to target task T_i is also high, i.e., $V^\pi(\rho_i, T_i)$ is close to $V^\pi(\rho_j, T_j)$, then Proposition 1 implies that the transition functions p_i and p_j might be similar, as are the initial state distributions ρ_i and ρ_j. Consequently, if a source policy can achieve high zero-shot transfer success on a target task, the target task might have a similar transition function and initial state distribution as the source task. Hence, we hypothesize that fine-tuning the source policy on the target task will be efficient.

However, it is important to note that achieving a similarly high success rate on two tasks with a single policy does not necessarily indicate similar dynamics between the tasks. Proposition 1 establishes that similar dynamics and initial state distributions lead to similar expected values for a given policy, but the reverse is not guaranteed. We use the high transfer success rate as a heuristic indicator of similar dynamics, serving as intuitive motivation rather than strict theoretical justification.

A.3 METHOD

Algorithm 1 Policy finetuning with Self-imitation Learning

Initialize parameter θ for policy π_θ and value function V_θ with retrieved skill
Initialize replay buffer $\mathcal{D} \leftarrow \emptyset$
Initialize episode buffer $\mathcal{E} \leftarrow \emptyset$
for each iteration **do**
  # Collect training samples
  for each step **do**
    Execute an action $s_t, a_t, r_t, s_{t+1} \sim \pi_\theta(a_t|s_t)$
    Store transition $\mathcal{E} \leftarrow \mathcal{E} \cup \{(s_t, a_t, r_t)\}$
  end for
  if s_{t+1} is terminal **then**
    # Update replay buffer
    Compute returns $R_t = \sum_k^\infty \gamma^{k-t} r_k$ for all t in $\mathcal{E}$
    $\mathcal{D} \leftarrow \mathcal{D} \cup \{(s_t, a_t, R_t)\}$ for all t in $\mathcal{E}$
    Clear episode buffer $\mathcal{E} \leftarrow \emptyset$
  end if
  # Update parameter θ using PPO objective
  $\theta \leftarrow \theta - \eta \nabla_\theta \mathcal{L}^{ppo}$ (Schulman et al., 2017)
  # Perform self-imitation learning
  for $m = 1$ to M **do**
    Sample a mini-batch $\{(s, a, R)\}$ from $\mathcal{D}$
    $\theta \leftarrow \theta - \eta \nabla_\theta \mathcal{L}^{sil}$
  end for
end for

Algorithm 2 Continual Learning with Skill Library Expansion

Require: Prior tasks $\mathcal{T}_{prior} = \{T_1, T_2, \cdots, T_n\}$; Skill library $\Pi_{prior} = \{\pi_1, \pi_2, \cdots, \pi_n\}$
1: **while** given newly coming batch of tasks $\mathcal{T}^j = \{T_1, T_2, \cdots, T_k\}$ **do**
2: **for** each task T_i **do**
3: Retrieve a policy π_{src} from the skill library Π_{prior}
4: Finetune π_{src} to get a policy π_i solving the task T_i
5: Expand the skill library, $\mathcal{T}_{prior} = \mathcal{T}_{prior} \cup \{T_i\}$; $\Pi_{prior} = \Pi_{prior} \cup \{\pi_i\}$
6: **end for**
7: **end while**

A.4 Implementation Detail

A.4.1 Task Feature Learning in SRSA

Geometry Features As shown in Fig. 3(a), we employ a PointNet-based (Qi et al., 2017) autoencoder E_G and D_G to minimize the difference between input point cloud P and reconstructed point cloud $D_G(E_G(P))$. The autoencoder is trained using point clouds of parts from all tasks.

We follow the implementation details outlined in (Tang et al., 2024). In a large set of meshes M for various assembly parts, each mesh $m_i \in M$ consists of (V_i, E_i), where V denotes the vertices and E represents the (undirected) edges. During each training iteration, we sample a batch of meshes $B \subset M$. For each $m_i \in B$, we generate a point cloud P_i from the mesh, with each point located on the surface of m_i. The point cloud P_i ghdn is passed through a PointNet encoder (Qi et al., 2017) based on the implementation from (Mu et al., 2021) to produce a latent vector. The latent vector $z_{G,i}$ is subsequently fed into a fully-convolutional decoder, following the implementation from (Wan et al., 2023) to produce the reconstructed point cloud P_i'.

The network is trained to minimize reconstruction loss, defined here as the Chamfer distance between P_i and P_i':

$$\mathcal{L}_{CD} = \frac{1}{\|P_i\|} \sum_{p \in P_i} \min_{q \in Q_i} \|p - q\|_2^2 + \frac{1}{\|Q_i\|} \sum_{q \in Q_i} \min_{p \in P_i} \|p - q\|_2^2$$

Across 100 two-parts assembly tasks, we utilize a total of 200 meshes for the plug and socket components with $|M| = 200$. Each sampled point cloud P_i contains 2000 points and the dimension of learned embedding is $|z_{G,i}| = 32$. The autoencoder is trained for a total of 23,000 epochs, using a batch size of 64 and a learning rate of 0.001.

To represent the feature of one task, we gather the geometry features for the meshes of plug, socket, and the assembled state of the plug inserted in the socket. Therefore, the geometry feature of one task is concatenation of these three features, resulting in a dismensionality of, $|z_{G,i}| = 96$.

Dynamics Features We build upon prior work in context-based meta-RL (Rakelly et al., 2019; Lee et al., 2020) to utilize a context encoder E_D that produces a latent vector from transition segments $\tau_{t-1} = \{s_{t-h}, a_{t-h}, s_{t-h+1}, a_{t-h+1}, \cdots, s_{t-1}, a_{t-1}\}$, as shown in Fig. 3(b). We sample the transition segments from disassembly trajectories, compute the latent vector $E_D(\tau_{t-1})$, and feed the latent vector from transition segments to a forward dynamics model D_D across all tasks. For any transition samples from any task, the forward dynamics model is trained to predict the next state $s_{t+1}' = D_D(E_D(\tau_{t-1}), s_t, a_t)$ to be close to the ground-truth next state s_{t+1}.

As described in (Tang et al., 2024), for each task, we generate disassembly paths by initializing the robot hand to grasp the plug in the assembled state, where the plug is fully inserted in the socket. Using a low-level controller, we lift the plug from the socket and move it to a randomized pose. We repeat this process until collecting 100 successful disassembly trajectories. We store the state of end-effector position and the action of moving end-effector at each timestep in the disassembly trajectories. Each task has a total of 100 disassembly trajectories, with each trajectory spanning 128 timesteps.

We sample the transition segment $\tau_{t-1} = \{s_{t-h}, a_{t-h}, s_{t-h+1}, a_{t-h+1}, \cdots, s_{t-1}, a_{t-1}\}$ for $h = 10$ timesteps. The context encoder is modeled as multi-layer perceptrons (MLPs) with 3 hidden layers of sizes $(256, 128, 64)$, producing a 32-dimensional vector $z_{D,t}$. Then, the forward dynamics model D_D receives the context vector as an additional input, where the input consists of a concatenation of state s_t, action a_t, and context vector $z_{D,t}$. The forward dynamics model comprises four fully-connected layers of sizes $(200, 200, 200, 200)$ with ReLU activation functions, outputing the prediction of the next state s_{t+1}'. The objective is to minimize L2-distance between the ground-truth next state s_{t+1} and the predicted next state s_{t+1}'. For the entire set of disassembly trajectories across 100 tasks, we train the encoder and forward dynamics model for 200 epochs, using a batch size of 128 and a learning rate of 0.001.

Expert Action Features We utilize the disassembly trajectories as reverse expert demonstrations for assembly tasks and aim to capture expert action information in an embedding space. As illustrated in Fig. 3(c), we sample a transition segment τ_{t-1} from the disassembly trajectories, map it

to the action embedding $E_A(\tau_{t-1})$, and reconstruct the action sequence $\{a_{t-h}, a_{t-h+1}, \cdots, a_{t-1}\}$ using decoder D_A. We train both the encoder and decoder with transition segments from all tasks. This embedding effectively extracts the strategy for solving the task by reconstructing the expert actions from the disassembly trajectories.

We sample the transition segment $\tau_{t-1} = \{s_{t-h}, a_{t-h}, s_{t-h+1}, a_{t-h+1}, \cdots, s_{t-1}, a_{t-1}\}$ for 10 timesteps (i.e., $h = 10$). The action encoder E_A is modeled as multi-layer perceptrons (MLPs) with three hidden layers of sizes $(256, 128, 64)$, producing a 32-dimensional vector $z_{A,t}$. The action decoder D_A is an MLP with four hidden layers of sizes $(200, 200, 200, 200)$ that predicts the sequence of expert actions $\{a'_{t-h}, a'_{t-h+1}, \cdots, a'_{t-1}\}$. We minimize the L2-distance between input action sequence $\{a_{t-h}, a_{t-h+1}, \cdots, a_{t-1}\}$ and the reconstructed action sequence $\{a'_{t-h}, a'_{t-h+1}, \cdots, a'_{t-1}\}$. The encoder and decoder are trained for 200 epochs, using a batch size of 128 and a learning rate of 0.001.

A.4.2 Transfer Success Prediction in SRSA

We learn the function $F(\pi_{src}, T_{trg})$ to predict the transfer success. For any pair of source policy and target task in the skill library, we execute the source policy in the target task for 1000 episodes and average the success rate to obtain the ground-truth label for F. For any task T in the prior task set, we sample the point cloud P_i of plug, socket and assembly state to extract the geometry feature $z_{G,i}$ with a dimension of 96. Then we sample transition segment τ_i to obtain the dynamics feature $z_{D,i}$ with a dimension of 32 and action feature $z_{A,i}$ with a dimension of 32. By concatenating these features, we create a task feature z_i with a dimension of 160 for the sampled point clouds and transition segment. With both the task features $z_{src,i}$ and $z_{trg,i}$ for source and target tasks, we feed them into an MLP with one hidden layer of size 128 to predict the transfer success. We optimize the MLP while jointly finetuning the feature encoders E_G, E_D, and E_A to learn the transfer success prediction. The training is conducted for 50 epochs across all source-target pairs in the prior task set.

A.4.3 Baselines of Skill Retrieval Approaches

Signature : path signature can represent trajectories as a collection of path integrals and also quantify distances between trajectories. Inspired by (Tang et al., 2024), we find the closest path signature for skill retrieval. For each disassembly trajectory τ_k on the target task T, we calculate the path signature z_k and search all disassembly trajectories over all source tasks to identify a source disassembly trajectory τ_j with the path signature z_j closest to z_k. The source disassembly trajectory τ_j belongs to a source task in $\mathcal{T}_{prior}$, and thus we match the target trajectory τ_k to this source task, denoted as T_k. We count the times that one source task $T_{src} \in \mathcal{T}_{prior}$ is assigned as the source task for a target disassembly trajectory, $C(T_{src}) = \sum_{k=1}^{n} [T_k = T_{src}]$. Then we retrieve the source policy for one source task with the highest count, i.e. $\arg\max_{T_{src}} C(T_{src})$

Behavior : Inspired by (Du et al., 2023), we employ state-action pairs on disassembly trajectories across all tasks and learn a state-action embedding with a VAE for skill retrieval. For any state-action pair (s_k, a_k) on the target task, we infer the embedding $z_{sa,k}$ and look for one state-action pair (s_j, a_j) from the disassembly trajectories in source tasks with the embedding $z_{sa,j}$ closest to $z_{sa,k}$. The target state-action pair (s_k, a_k) is matched to one source task, which (s_j, a_j) belongs to. We denote this source task as T_k. Similar to the method above, we count the times that one source task $T_{src} \in \mathcal{T}_{prior}$ is assigned as the source task for a target state-action pair, $C(T_{src}) = \sum_{k=1}^{n} [T_k = T_{src}]$. Then we retrieve the source policy for one source task with the highest count, i.e. $\arg\max_{T_{src}} C(T_{src})$

Forward : As explained above, we learn the latent vector for transition sequence τ on disassembly trajectories. In order to retrieve one source task according to the distances between task embeddings, we average embedding for all transition sequences from the same task to obtain the task embedding, similar to (Guo et al., 2022). We retrieve the policy for the source task that has the closest task embedding.

Hyperparameters	Value
Policy Network Architecture	[256, 128, 64]
Value Function Architecture	[256, 128, 64]
LSTM network size	256
Horizon length (T)	32
Adam learning rate	1e-4
Discount factor (γ)	0.99
GAE parameter (λ)	0.95
Entropy coefficient	0.0
Critic coefficient	2
Minibatch size	8192
Minibatch epochs	8
Clipping parameter (ϵ)	0.2
LSTM network size	256
SIL update per iteration	1
SIL batch size	8192
SIL loss weight	1
SIL value loss weight (β)	0.01
Replay buffer size	10^5
Exponent for prioritization	0.6

Table 1: Hyperparameters in PPO and Self-imitation learning

Geometry : As explained above, we learn an autoencoder for the point clouds of the assembly assets to minimize the reconstruction loss, as conducted in (Tang et al., 2024). We retrieve the policy for the source task with the closest point-cloud embedding.

A.4.4 Skill Adaptation in SRSA

Following (Tang et al., 2024), we use PPO to train the stochastic policy π_θ (i.e., actor) and an approximation of the value function V_θ (i.e., critic), parameterized by a neural networks with weights θ. While the policy is stochastic following a multivariant normal distribution with the learned mean and standard deviation, at evaluation and deployment time, the action output from well-trained policy is deterministic.

The input state for the policy network consists of the robot arm's joint angles, the end-effector pose, the goal end-effector pose, and the relative pose of the end effector to the goal. The state has a dimensionality of 28.

Due to the asymmetric actor-critic strategy, the states provided to the value function include privileged information not available to the policy. The states for the critic include joint velocities, end-effector velocities, and the plug pose, resulting in an input dimensionality of 44 for the value function.

The action space consists of incremental pose targets, representing the position and orientation differences between the current pose and the target pose. We use incremental targets instead of absolute targets to restrict selection to a small, bounded spatial range. The action dimensionality is 6.

SRSA combines PPO with a self-imitation learning mechanism for policy fine-tuning. We maintain a replay buffer $\mathcal{D}$ for transitions encountered during training, defined as $\mathcal{D} = \{s_i, a_i, R_i\}$. The data samples in the buffer are prioritized based on the discounted accumulated reward.

As shown in Algorithm 1, each iteration includes one PPO update for the policy and value function, along with a batch sampling from $\mathcal{D}$ to perform one self-imitation learning update. This update aims to minimize the loss function $\mathcal{L}_{sil}$ defined in Sec. 4.2. For details on network architectures and hyperparameters, refer to Tab. 1.

We follow prior work to use object poses rather than visual observations as input to the policy. Incorporating vision-based observations would introduce additional challenges for zero-shot sim-to-real transfer, as it requires a camera. In contrast, the current policy only relies on the fixed socket pose and the robot's proprioceptive features (including the end-effector pose), making it more straightforward to execute the policy in real-world settings. Using visual observations or object pose

is orthogonal to our proposed method (i.e., SRSA is independent of the observation modality). The idea of retrieving a relevant skill and fine-tuning the retrieved policy may also be useful if the policy has visual observation input.

A.5 EXPERIMENTS

A.5.1 SKILL RETRIEVAL

We first replicate the specialist policy learning for 100 assembly tasks as described in (Tang et al., 2024). Then, these 100 tasks are split into 90 prior tasks and 10 test tasks. For the 90 prior tasks, we use the well-trained specialist policies to build the skill library.

We train the skill-retrieval method on the prior tasks and evaluate its performance on the test tasks. In Fig. 4 in main text, 11, and 12 in Appendix, we present the test results for three different ways of splitting the 100 tasks. Overall, SRSA demonstrates superior performance in identifying relevant policies from the skill library, achieving a high success rate in zero-shot transfer.

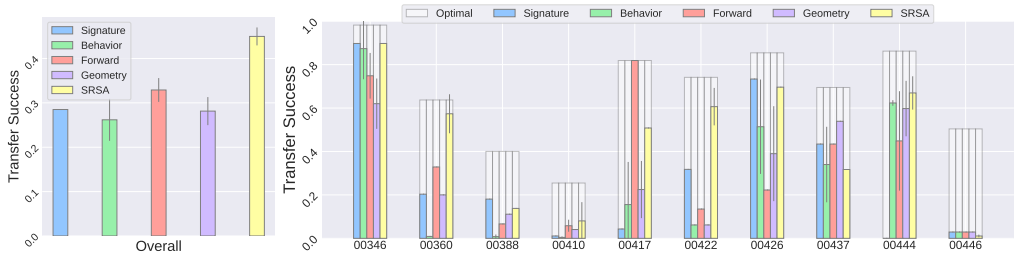

Figure 11: **Transfer success of retrieved skills applied to test tasks**. For each of the test tasks, we retrieve a policy from the prior skill library using 5 different approaches. For each approach, if it involves training neural networks, we train it for 3 random seeds. **Left**: we illustrate the mean result over 10 test tasks. **Right**: For each test task, we show the mean and standard deviation of transfer success over 3 seeds. Overall, SRSA clearly outperforms baselines.

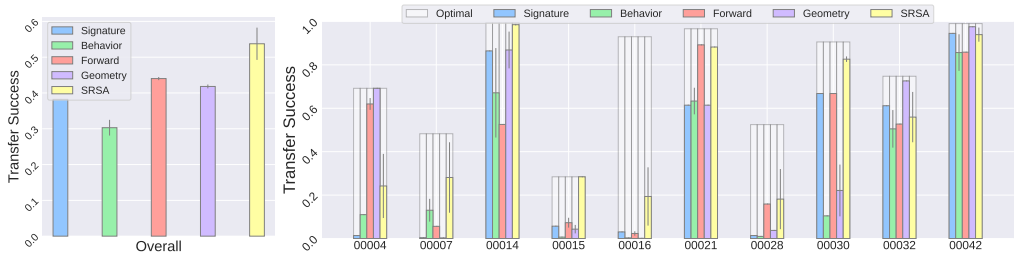

Figure 12: **Transfer success of retrieved skills applied to test tasks**. For each of the test tasks, we retrieve a policy from the prior skill library using 5 different approaches. For each approach, if it involves training neural networks, we train it for 3 random seeds. **Left**: we illustrate the mean result over 10 test tasks. **Right**: For each test task, we show the mean and standard deviation of transfer success over 3 seeds. Overall, SRSA clearly outperforms baselines.

A.5.2 SKILL ADAPTATION

We show the learning curves in Fig. 5 in main text. At the end of 1000 training epochs, we record the success rate of the learned policies on 10 test tasks. For AutoMate, the policies are learned from scratch using PPO on the 10 test tasks. In contrast, SRSA initializes the policies with retrieved skills and fine-tunes them using PPO combined with self-imitation learning. The retrieval mechanism is trained on a skill library of 90 prior tasks, where the skills were pre-trained by AutoMate.

Compared to the baseline success rate of 69.4%, SRSA achieves a significantly higher success rate of 84.7%, corresponding to an absolute improvement of 15.3 percentage points and a relative improvement of approximately 22.0%. By leveraging the knowledge from the skill library, SRSA also

obtains 3.7x lower standard deviation compared to AutoMate (Tab. 2). This advantage becomes even more pronounced in sparse-reward scenarios, where SRSA shows an absolute improvement of 41.9 percentage points and a relative improvement of 139% in comparison with baseline. (Tab. 3).

Task ID	01029	01036	01041	01053	01079	01092	01102	01125	01129	01136	Average
AutoMate	53.4 (27.4)	89.0 (7.7)	79.1 (8.4)	49.1 (15.3)	74.3 (32.9)	59.4 (13.1)	76.4 (11.4)	49.6 (3.2)	76.0 (3.0)	87.3 (4.2)	69.4 (12.7)
SRSA	98.5 (0.4)	91.3 (6.0)	83.3 (4.4)	75.4 (6.4)	93.60 (3.6)	78.3 (6.3)	92.5 (0.5)	50.6 (1.6)	85.8 (4.0)	98.4 (0.4)	84.7 (3.4)

Table 2: **Mean (standard deviation) of success rate (%) on each test task, in dense-reward setting**. We calculate the mean and standard deviation over 5 runs of different random seeds, at the last training epoch (i.e. 1000 epochs).

Task ID	01029	01036	01041	01053	01079	01092	01102	01125	01129	01136	Average
AutoMate	61.3 (26.5)	37.2 (31.4)	14.4 (1.6)	0 (0.5)	81.7 (15.1)	0 (0.5)	1.4 (1.0)	9.8 (2.0)	55.6 (6.0)	39.7 (5.4)	30.1 (9.0)
SRSA	95.1 (1.1)	78.7 (8.9)	33.7 (6.4)	92.5 (2.2)	96.1 (1.7)	51.4 (5.5)	70.7 (2.9)	51.2 (9.3)	90.3 (7.2)	60.5 (2.6)	72.0 (4.8)

Table 3: **Mean (standard deviation) of success rate (%) on each test task, in sparse-reward setting**. We calculate the mean and standard deviation over 5 runs of different random seeds, at the last training epoch (i.e., 1000 epochs).

A.5.3 Continual Learning

We begin with an initial skill library containing 10 policies and expand its size by 10 policies per round over 9 rounds, eventually reaching 100 policies. When the skill library contains fewer than 40 policies, the number of source-target task pairs from the prior task set is limited. During this phase, we retrieve skills solely based on geometry embeddings. Once the skill library reaches 40 or more policies, we train the transfer success prediction function F to guide skill retrieval for new tasks.

In the continual learning setting, Fig. 8 in main text and Fig. 13 in Appendix show the efficiency of SRSA and AutoMate under two different task batch orderings. In both cases, SRSA demonstrates significantly better sample efficiency compared to AutoMate.

Additionally, we compare SRSA and AutoMate based on the best checkpoint, measured by the highest rewards achieved over 5 runs for each task. In our replication of AutoMate, we achieved an average success rate of 70% across 100 assembly tasks, which is lower than the 80% reported in the original paper. This discrepancy may be due to differences in simulator versions, asset meshes, implementation details, and other factors.

On average, SRSA achieves a success rate of 79% in Fig. 14 and 73% in Fig. 15, for two cases of task ordering, respectively. SRSA demonstrates a higher success rate and better sample efficiency than the baseline AutoMate.

A.5.4 Ablation Study

Fig. 16 illustrates the learning curves of different SRSA variations across 10 test tasks.

Skills retrieved based solely on geometry embeddings may face challenges during adaptation due to dynamic differences between the source and target tasks. As a result, the learning curves of SRSA-Geom tend to be less efficient and more unstable than SRSA.

When self-imitation learning is removed (SRSA-noSIL) from SRSA, the learning curves show increased fluctuation and higher variance across runs.

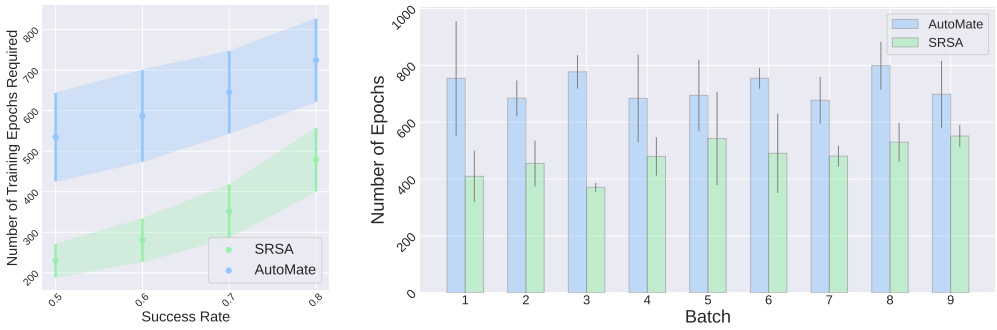

(a) (b)

Figure 13: **(a) Sample efficiency of policy learning in a continual-learning setting**. We report how many training epochs are required to reach desired success rates (0.5, 0.6, 0.7, 0.8). We calculate the mean and standard deviation of training epochs over 5 runs, and report the average over 90 tasks.**(b) Number of training epochs required for different batches**. In the continual-learning scenario, we proceed through 9 batches of new tasks for policy learning, with each batch containing 10 new tasks. For each batch, we show the mean and standard deviation of training epochs required to reach a success rate of 0.8. SRSA requires less number of training epochs to reach a good success rate.

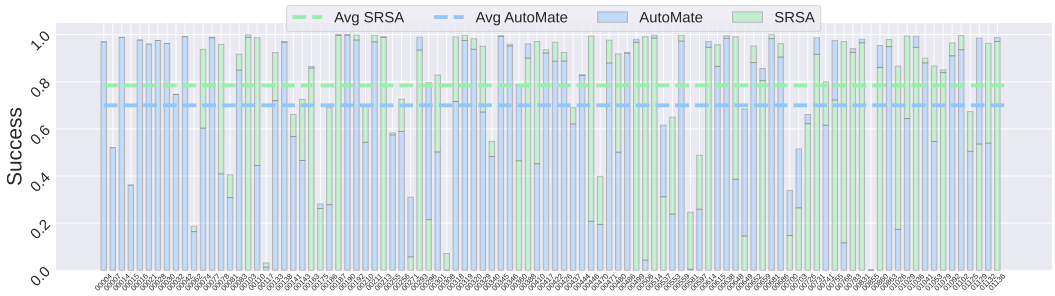

Figure 14: **Comparison of SRSA and AutoMate success rate over 100 tasks**. We replicate the specialist policy learning in the AutoMate paper over all tasks, and run SRSA with the continual-learning approach to train 90 specialist policies with initial skill library of 10 policies. For both approaches, for each task, we select the best checkpoint among 5 runs with different random seeds. We compare the success rate on all the tasks. On average, SRSA achieves a higher success rate.

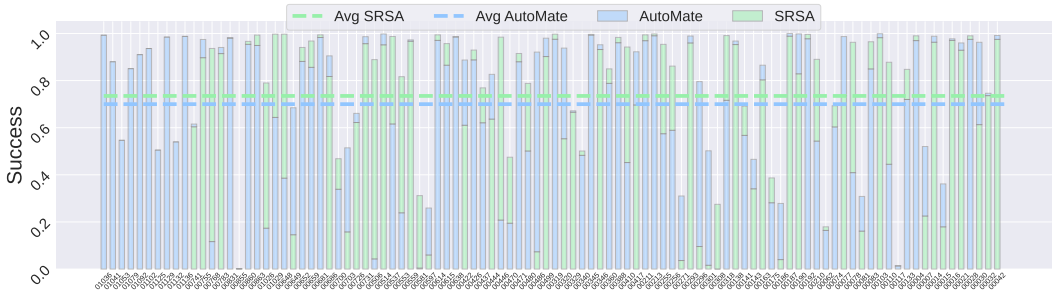

Figure 15: **Comparison of SRSA and AutoMate success rate over 100 tasks**. We replicate the specialist policy learning in the AutoMate paper over all tasks, and run SRSA with the continual-learning approach to train 90 specialist policies with the initial skill library of 10 policies. For both approaches, for each task, we select the best checkpoint among 5 runs with different random seeds. We compare the success rate on all the tasks. On average, SRSA achieves a higher success rate.

For the generalist policy, which was trained on 20 tasks from AutoMate (including tasks 01036, 01041, 01129, 01136), fine-tuning on these tasks yields strong performance since the policy was

already optimized for them. However, on other test tasks, the generalist policy is not as effective for efficient policy learning compared to the skills retrieved by SRSA.

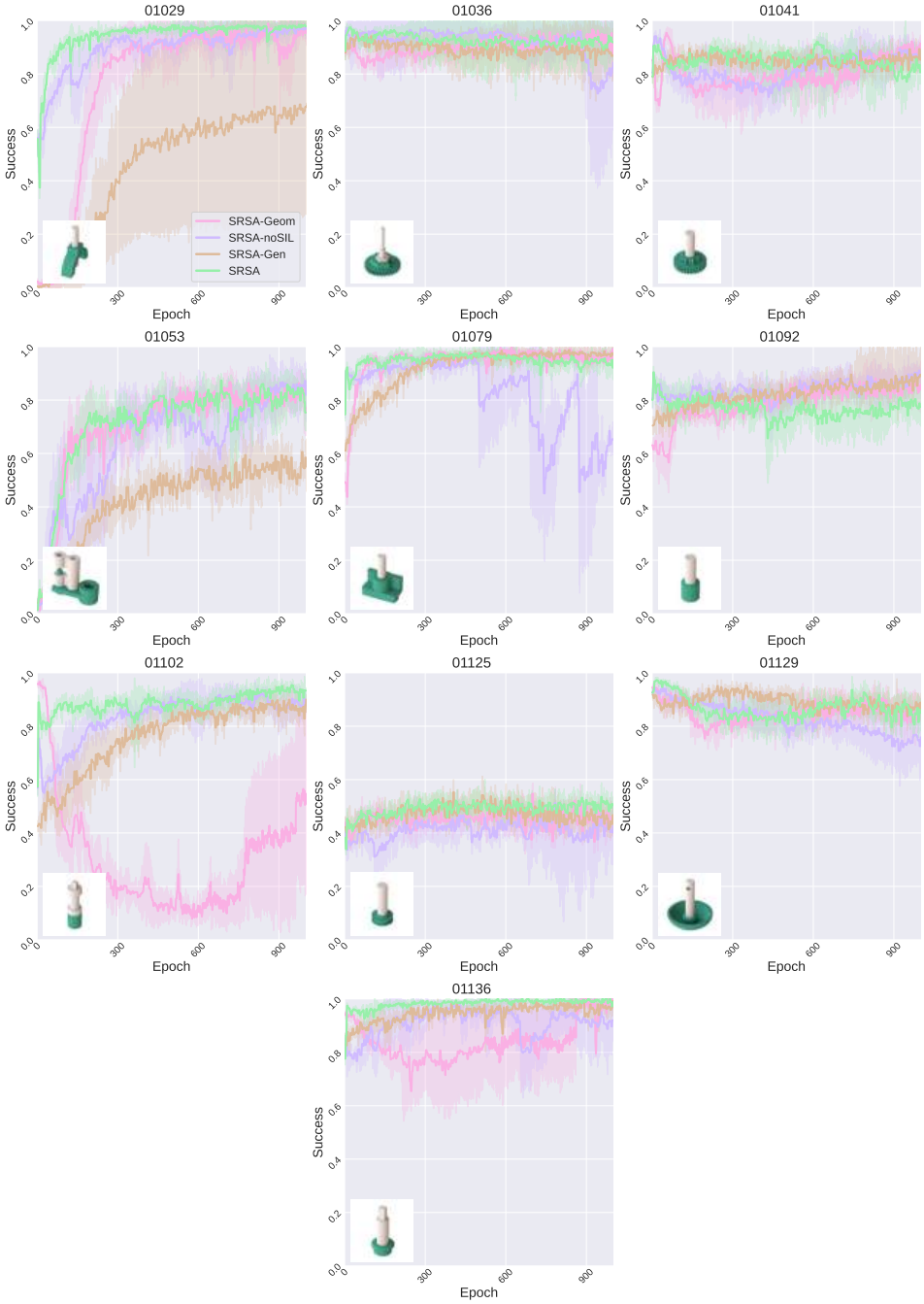

Figure 16: **Comparison for variants of SRSA with different ablated components**. For each method, we have 5 runs with different random seeds. The learning curves show mean and standard deviation of success rate over these runs.

Fine-tuning a state-based generalist policy does not perform well because the generalist policy has limited capacity and it cannot cover more than 20 training tasks.

Fine-tuning a vision-based generalist policy presents additional challenges, such as effectively learning a generalist policy across multiple prior tasks with high-dimensional vision observations, fine-tuning on new tasks without forgetting prior ones, and addressing continual learning scenarios, in-

cluding whether to fine-tune the original generalist policy or one already fine-tuned on other tasks. To further investigate the reviewer's inquiry, we made an initial attempt to train a vision-based generalist policy with PPO and fine-tune it. Given 90 prior tasks, it can only reach around 10% average success rate after training for two days. We expect such a generalist policy would perform no better than random initialization when fine-tuned for new tasks. Vision-based RL for generalist policy on assembly tasks is a relevantly new topic, and the development of such policies lies beyond the scope of SRSA. We leave this direction for future research.

A.6 Comparison with Geometry-based Retrieval

During adaptation, the final performance of SRSA-geom looks close to SRSA in some cases (see Fig. 16). However, it is statistically worse than SRSA, especially when there is a smaller number of training epochs. To provide a more comprehensive evaluation, we run SRSA-geom and SRSA across additional target tasks with three random seeds. The table below summarizes statistics of success rate at different numbers of training epochs, showing that SRSA consistently achieves higher success rates with lower variance. In industrial settings, a 3–9% difference in success rate can be significant.

	Test task set 1		Test task set 2	
Success rate (%)	Epoch 500	Epoch 1000	Epoch 500	Epoch 1000
SRSA-geom	73.6 ($\pm$ 6.9)	81.0 ($\pm$7.7)	67.7($\pm$7.1)	71.4($\pm$8.1)
SRSA	**82.8($\pm$4.2)**	**84.3($\pm$3.4)**	**76.2($\pm$3.0)**	**77.6($\pm$3.5)**

Geometry-based retrieval alone is not always sufficient. When tasks share similar geometry but have different dynamics, SRSA-geom struggles to transfer as effectively as SRSA.

For example, for the target task 01092, SRSA-geom retrieves source task 00686, achieving a transfer success rate of only 61.1%, whereas SRSA retrieves task 00213 with a higher success rate of 76.7%. While the overall shapes of 01092 and 00686 are similar (see below), the lower part of plug in task 01092 is thinner than the upper part, and there is only a short distance to insert this lower part into the socket. These features closely resemble task 00213, i.e., a narrow plug to be inserted a short distance to accomplish assembly. These shared physical characteristics and similar task-solving strategies make 00213 better suited for transfer. In assembly tasks, the dynamics of the contact region are often more critical than overall geometry for task success. Therefore, source task 00213 works better than 00686 when transferring to the target task 01092.

(a) Assembly tasks in the first example (b) Assembly tasks in the second example

Additionally, we examine assembly tasks with identical geometry but differing physical parameters. For instance, consider the target task 01136 with a friction value of 10.0. One source task has the same geometry as 01136 but a significantly lower friction value of 0.5. SRSA-geom selects this source task due to its geometric similarity; however, the corresponding source policy achieves only 88.9% transfer success on the target task, due to the friction mismatch (despite achieving a 99.3% success rate on its original source task). In contrast, SRSA selects the source task 00213, whose policy better aligns with the target task's dynamics, resulting in a higher transfer success rate of 93.2%

A.7 Analysis of Source Policy Success as Input for Retrieval

The success rate of the source policy on the source task is meaningful information to represent the source policy. To see whether it is practically beneficial for retrieval, we modify our approach. We simply concatenate this source success rate information with the task features of source and target tasks. We train the transfer success predictor F with these features as inputs.

We consider three random splits between the prior task set (90 tasks) and test task set (10 tasks). For each split, we train F on the prior task set over three random seeds. For each seed, we test the trained function F on the test task set for retrieval. We report the mean transfer success rate of the retrieved skills on 10 test tasks, with the standard deviation reported over three seeds. Empirically, the source success rate as input to F only slightly improves the retrieval results.

Average transfer success (%)	Test task set 1	Test task set 2	Test task set 3
SRSA	62.7 (+-5.7)	53.7 (+-5.5)	**44.9 (+-2.4)**
SRSA+source success rate	**66.7 (+-0.3)**	**53.7(+-2.6)**	**43.7 (+-3.7)**

A.8 Analysis of Out-of-Distribution Test Tasks

For out-of-distribution (OOD) tasks where no skill transfers zero-shot, SRSA may indeed struggle, and the initialization from a retrieved skill might not help much. To tackle this, it's essential to build a skill library that's as diverse as possible. When the target task falls outside the current library's distribution, we can use SRSA's continual learning approach (section 4.3 & 5.4) to expand the library with new tasks. By building a larger, more varied skill library, we increase the likelihood that this target task will align better with tasks in the skill library.

We run experiments for target tasks with IDs 00004, 00015, 00016, 00028, 00030. These tasks suffer from low transfer success rate given a small skill library with only 10 prior tasks. However, when we have a larger and larger skill library, the retrieved skill has a higher transfer success rate on the target task.

Transfer success rate (%)	00004	00015	00016	00028	00030
10-task library	15.9	6.9	0.2	12.2	39.1
50-task library	12.7	8.4	0.3	**27.5**	49.4
90-task library	**24.2**	**28.4**	**19.3**	18.1	**82.6**

As demonstrated, continual learning to expand the skill library is a promising step; however, generalizing to OOD tasks is a longstanding challenge in robotics, and it is still an open question how to optimally construct the curriculum that governs the expansion of the skill library.

A.9 Analysis of Other Metrics for Retrieval

We acknowledge that zero-shot transfer success rate may not be a perfect proxy for retrieval. We can consider several other possible metrics for retrieval: (1) Ground-truth success rate after adaptation (2) Predicted success rate after adaptation (3) Predicted success rate in zero-shot manner (i.e. SRSA) (4) Predicted dense rewards in zero-shot manner.

Option 1 is the ideal metric to identify the best skill for retrieval, as our final goal is to obtain the highest success rate on the target task after adaptation. However, it introduces a chicken-and-egg problem, as we cannot get this metric without fine-tuning all candidate policies on the target task.

Option 2 requires training a predictor for the success rate after adapting any source policy on any target task. We need the training labels of the ground-truth success rate after adaptation. Unfortunately, collecting this training data would require extensive computational resources. For each source-target pair, we need at least 20 GPU hours to finish adaptation; given a skill library of 100 tasks, 200,000 GPU hours would be required to collect training data. Furthermore, it will remain intractable as the skill library becomes larger.

Option 3 (SRSA) requires much less resources to collect training data for the predictor. We only need 20 minutes on a GPU to evaluate one source policy on a target task. It thus requires 3,000 GPU hours to collect training labels. We conduct an experiment to compare the performance of Option 1 and Option 3 on two test tasks. To collect experimental results for Option 1, for each test task, we sweep all 90 source policies in our skill library. We finetune each source policy with one random seed to adapt to the target task and identify the best success rate after adaptation. We only afford the computational resources for two test tasks to sweep fine-tuning for Option 1. Below we report the success rate of Option 1 and Option 3 after fine-tuning for 1500 epochs

Success rate after adaptation (%)	Test task 1036	Test task 1041
Option 3 (SRSA)	95.9	89.1
Option 1	98.3	94.0

Option 1 is the perfect but intractable metric for retrieval. The difference of success rate between the SRSA-retrieved skill (Option 3) and the best source skill (Option 1) is less than 5% after adaptation. Therefore, although zero-shot transfer success rate is not a perfect metric for retrieval, it is a high-quality metric for retrieval in terms of both performance and computational efficiency.

Furthermore, we consider using dense reward information to guide retrieval (Option 4). We learn to predict the accumulated reward rather than success rate on the target task when executing the source policies in a zero-shot manner; then we retrieve the source policy with the highest predicted transfer reward. In the table below, we show the performance of retrieved skills when they are applied on the target tasks.

	Test task set 1		Test task set 2	
	Transfer reward	Transfer success (%)	Transfer reward	Transfer success (%)
Option 3 (SRSA)	**8134**	**62.7**	7722	**53.7**
Option 4	7976	54.8	**7935**	32.6

In the AutoMate task set, Option 3 (SRSA) yields slightly better skill retrievals, especially with higher transfer success on the target task. However, success rate may not accurately reflect the expected value for tasks with dense rewards. The higher transfer success rate does not mean higher transfer reward in test task set 2. Therefore, if it is critical to prioritize the reward achieved on the target task, using the transfer-reward predictor for retrieval is a reasonable choice. Conversely, if the success rate on the target task is more critical (as in our assembly tasks), the transfer success would be the preferred choice as a retrieval metric.

A.10 Analysis of Distance Metrics for Task Features

We concatenate the features of geometry, dynamics and expert actions as the task features, and apply some distance metrics between the vectors as the metrics for retrieval. We consider three different ways to split the prior task set (90 tasks) and test task set (10 tasks). We consider L2 distance, L1 distance, and negative cosine similarity as distance metrics. For each test task, we retrieve the source task with the closest task feature to the target task. However, the retrieval result is worse than SRSA on three different test task sets.

Transfer success rate (%)	L2 distance	L1 distance	Cosine similarity	SRSA
Test task set 1	51.6	50.8	52.6	**62.7**
Test task set 2	47.1	49.0	46.5	**53.7**
Test task set 3	35.3	35.0	36.1	**44.9**

We jointly learn features from geometry, dynamics and expert actions to represent tasks, and predict transfer success to implicitly capture other transfer-related factors from tasks. SRSA learning function F aims to capture additional information for transfer success prediction. Therefore, the prediction function F provides a better metric to identify the source task with higher zero-shot transfer success.

A.11 Ablation Study on Policy Initialization and Self-Imitation Learning

As for policy learning, AutoMate is PPO from random policy initialization, and SRSA is PPO with self-imitation learning (SIL) after initialization with the retrieved skill. Thus, the main difference between SRSA and AutoMate lies in (1) strong initialization from retrieval and (2) SIL. In section 6, we compared SRSA and SRSA-noSIL to show the effect of SIL. Below, we additionally compare with SRSA with random initialization (SRSA-noRetr) to show the effect of initialization from retrieval.

Comparing AutoMate with SRSA-noRetr, we see the difference between PPO and PPO+SIL when learning a policy from scratch. Both approaches started from poor performance, but SIL has greater learning efficiency and stability. Comparing SRSA-noRetr and SRSA, we see the difference between

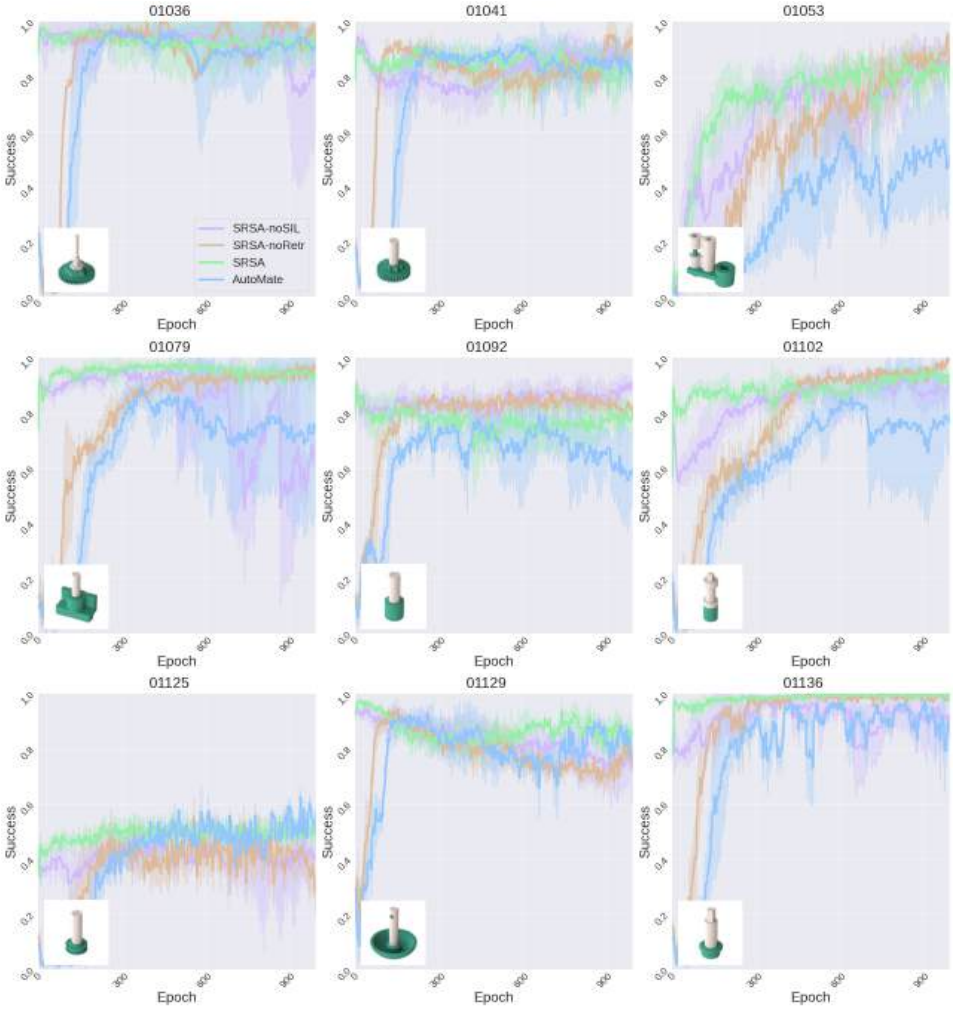

Figure 17: **Comparison for variants of SRSA with different ablated components**. For each method, we have 5 runs with different random seeds. The learning curves show mean and standard deviation of success rate over these runs.

random initialization and initialization from retrieval. Policy retrieval provides a good start with a reasonable success rate. As a result, SRSA more efficiently reaches higher performance on the target task.